ANALYSIS OF TARGET MODELS AND EVALUATION OF DETECTION CAPABILITY FOR DIFFERENT FALSE ALARM RATE IN PRESENCE OF FLUCTUATING TARGETS USING SWERLING MODEL IN RADAR SYSTEM

MD. MAYNUL ISLAM
(BSc Engg., MIST)

A THESIS SUBMITTED
FOR THE DEGREE OF MASTER OF SCIENCE
IN
ELECTRICAL, ELECTRONIC AND COMMUNICATION ENGINEERING

DEPARTMENT OF ELECTRICAL, ELECTRONIC AND COMMUNICATION ENGINEERING
MILITARY INSTITUTE OF SCIENCE AND TECHNOLOGY

2019

APPROVAL CERTIFICATE

The thesis titled **"Analysis of Target Models and Evaluation of Detection Capability for Different False Alarm Rate in Presence of Fluctuating Targets using Swerling Model in Radar System"** Submitted by Md. Maynul Islam, Roll No: 1014160017 (P) Session: 2014-15, has been accepted as satisfactory in partial fulfillment of the requirement for the degree of Master of Science in Electrical, Electronic and Communication Engineering on 20 January 2019.

BOARD OF EXAMINERS

1. _____
   Air Cdre Md Hossam-E-Haider, PhD — Chairman (Supervisor)
   Professor
   Department of EECE, MIST, Dhaka - 1216

2. _____
   Brig Gen A K M Nazrul Islam, PhD — Member (Ex-officio)
   Head
   Department of EECE, MIST, Dhaka - 1216

3. _____
   Lt Col Md. Tawfiq Amin, PhD — Member (Internal)
   Instructor Class A
   Department of EECE, MIST, Dhaka - 1216

4. _____
   Dr. Satya Prasad Majumder — Member (External)
   Professor
   Department of EEE, BUET, Dhaka - 1205

DECLARATION

I hereby declare that this thesis is my original work and it has been written by me in its entirety. I have duly acknowledged all the sources of information which have been used in the thesis.

This thesis has also not been submitted for any degree in any university previously.

_____

MD. MAYNUL ISLAM

20 January 2019

DEDICATION

To my Parents

ACKNOWLEDGEMENTS

It's an immense pleasure to express my profound gratitude to my respected supervisor Air Cdre Md Hossam-E-Haider, PhD for providing me the opportunity to work under him. I am grateful to him for his continuous guidance, kind help and wholehearted support during the work. Dr. Haider has had a tremendous impact on the way I perceive the research. His feedback from different critical angles has always been encouraging and very much useful.

My sincere gratitude and thanks to Brig Gen A K M Nazrul Islam, PhD, Head, EECE department. Without his kind support and valuable direction, it would not be possible for me to complete this research work.

As the program coordinator of post graduate program Lt Col Md. Tawfiq Amin, PhD helped me a lot. I would be pleased to extend my gratitude for his kind cooperation.

My special thanks to all my course teachers, faculties and staffs of EECE department, MIST. I am deeply thankful to my friends and colleagues of ICT department, BUP for their continuous inspiration.

My wholehearted thanks to each member of my family for being understanding and supportive. I am grateful to my parents for their continuous encouragement and support in every sphere of my life. My mother - the most caring person in this world gives me enormous mental support all the time. I cannot express my gratitude to her in words.

Finally, I would like to express my heartiest gratitude to Almighty Allah, the most Benevolent, the most Merciful. His blessings have brought me smooth accomplishment of this research.

Md. Maynul Islam
Military Institute of Science and Technology
Dhaka, Bangladesh
January, 2019

TABLE OF CONTENTS

APPROVAL CERTIFICATE ..... **i**
DECLARATION ..... **ii**
ACKNOWLEDGEMENTS ..... **iv**
TABLE OF CONTENTS ..... **v**
ABSTRACT ..... **viii**
LIST OF TABLES ..... **ix**
LIST OF FIGURES ..... **x**
LIST OF ABBREVIATIONS ..... **xii**
LIST OF SYMBOLS ..... **xiii**
CHAPTER ONE
INTRODUCTION **1**
1.1. Radar Fundamentals 1
1.1.1. Definition and basic function 1
1.1.2. Basic RADAR block diagram 2
1.1.3. Background of RADAR 3
1.1.4. Classification of RADAR 5
1.1.5. Radar frequency bands 6
1.2. Continuous Wave and Pulsed Radars 7
1.2.1. Continuous wave RADAR 7
1.2.2. Pulsed RADAR 7
1.3. Radar Terminologies 8
1.3.1. Pulse repetition frequency 8
1.3.2. Maximum unambiguous range 9
1.3.3. Range resolution 9
1.3.4. Doppler shift 11
1.3.5. Coherence 12
CHAPTER TWO
BRIEF OVERVIEW ON DETECTION CAPABILITY **13**
2.1. Introduction 13
2.2. Objective of the Thesis 13
2.3. Organization of the Thesis 13

2.4. Literature Review 14
2.4.1. Detection capability and false alarm rate 14
2.4.2. Probability of detection and CFAR loss in terms of threshold voltage 15
2.4.3. Reduction of side lobes using pulse compression technique 17
2.4.4. Atmospheric attenuation of Radar signal 17
2.5. Conclusion 18
CHAPTER THREE
ANALYSIS OF TARGET MODELS 19
3.1. Introduction 19
3.2. Signal Detection in Presence of Noise 19
3.3. Probability of False Alarm 22
3.4. Probability of Detection 23
3.5. Pulse Integration 23
3.5.1. Coherent integration 24
3.5.2. Non-Coherent Integration 24
3.6. Detection of Fluctuating Targets 25
3.6.1. Detection of probability density function 25
3.6.2. Threshold detection 26
3.7. Analysis of Probability of Detection 27
3.7.1. Target modelling 27
3.7.2. Chi-squared target models 28
3.7.3. Detection of Swerling I target 29
3.7.4. Detection of Swerling II target 29
3.7.5. Detection of Swerling III target 29
3.7.6. Detection of Swerling IV target 30
3.8. Cumulative Probability of Detection 30
3.9. Fundamentals of RADAR Equation 31
3.10. Constant False Alarm Rate (CFAR) 31
3.11. Cell-Averaging CFAR (single pulse) 32
3.12. Cell-Averaging CFAR with Non-Coherent Integration 33
3.13 Conclusion 34
CHAPTER FOUR
SIMULATION FOR EVALUATION OF SYSTEM PERFORMANCE 35
4.1. Introduction 35
4.2. Detection Capability in Presence of False Alarm Rate 36
4.3. Probability of Detection and CFAR Loss in terms of Threshold Voltage 36

4.4. Reduction of Side Lobes using Pulse Compression Technique 38
4.5. Atmospheric Attenuation of Propagated Radio Wave 41
4.6. Conclusion 43
CHAPTER FIVE
RESULTS AND DISCUSSIONS 44
5.1. Introduction 44
5.2. Detection Capability in Presence of False Alarm Rate 44
5.3. Probability of Detection and CFAR Loss in terms of Threshold Voltage 48
5.4. Reduction of Side Lobes Using Pulse Compression Technique 52
5.5. Atmospheric Attenuation of Propagated Wave 55
5.6. Conclusion 61
CHAPTER SIX
CONCLUSIONS AND FUTURE WORKS 62
6.1. Conclusions 62
6.2. Future Works 63
BIBLIOGRAPHY 64
LIST OF PUBLICATIONS 67
APPENDIX A-1

ABSTRACT

Target Detection is the most important factors in RADAR system and many researches have already done their research to improve the detection capability. This detection can be done for two types of targets, non-fluctuating targets and fluctuating targets. In practical cases, maximum targets are fluctuating in nature.

Analysis of false alarm rate can be a lead to the moderate value of threshold voltage. In this thesis, comparative analysis is carried out between probability of detection (P_d) and Constant False Alarm Rate (CFAR) for four different types of Swerling model. Conventional Cell Averaging CFAR is used here for the simulation.

In order to maintain a constant probability of false alarm the threshold value must be continuously updated based on the estimates of the noise variance. In this research, comparison is carried for CFAR loss versus gamma function for four types of Swerling model. Pulse compression is also introduced in this research by adding frequency modulation to a long pulse at transmission and by using a matched filter receiver in order to compress the received signal.

Further, performance analysis of detection capability of RADAR is found out for atmospheric attenuation in this research work by carrying out simulations with different system parameters. Comparison of results is also carried out with existing literature to validate the analytical approach.

LIST OF TABLES

Table 1.1. Frequency Band of RADAR 6
Table 5.1. System parameters 45
Table 5.2. Probability of Detection vs CFAR 47
Table 5.3. Side Lobes of Different Techniques 55

LIST OF FIGURES

Figure 1.1. Basic Radar Block Diagram. 3
Figure 1.2. Transmitter & Receiver of Radar. 8
Figure 1.3. PRF and IPP. 9
Figure 1.4. Range resolutions (a) Two unresolved targets, (b) Two resolved targets. .. 10
Figure 1.5. Effect of target motion on the reflected equi-phase waveforms. 10
Figure 1.6. Doppler shift due to moving radar and targets 11
Figure 1.7. (a) Phase continuity between consecutive pulses (b) Maintaining an integer multiple of wavelengths between the equi-phase wave fronts of any two successive pulses guarantees coherency. 12
Figure 3.1. Simplified block diagram of an envelope detector and threshold receiver. 20
Figure 3.2. Normalized detection threshold versus probability of false alarm. 22
Figure 3.3. Block diagram of a square law detector and non-coherent integration. 25
Figure 3.4. Threshold VT versus np for several values of nfa. 27
Figure 3.5. Detecting a target in many frames. 30
Figure 3.6. Conventional CA-CFAR. 32
Figure 3.7. Conventional CA-CFAR with non-coherent integration. 34
Figure 4.1. A block diagram of Analog Pulse Compression based on FFT and IFFT. . 39
Figure 4.2. Binary Phase Code of length 7. 40
Figure 4.3. Block diagram of barker code followed by a Transversal filter 41
Figure 5.1. Probability of Detection vs SNR(dB) for different number of pulses. 45
Figure 5.2.a. Probability of Detection vs CFAR for Swerling Model I. 46
Figure 5.2.b. Probability of Detection vs CFAR for Swerling Model II. 46
Figure 5.2.c. Probability of Detection vs CFAR for Swerling Model III. 47
Figure 5.2.d. Probability of Detection vs CFAR for Swerling Model IV. 47
Figure 5.3. CFAR Loss vs Gamma Parameter for Swerling Model I. 48
Figure 5.4. CFAR Loss vs Gamma Parameter for Swerling Model II. 49
Figure 5.5. CFAR Loss vs Gamma Parameter for Swerling Model III. 49
Figure 5.6. CFAR Loss vs Gamma Parameter for Swerling Model IV. 50
Figure 5.7. Pd vs Gamma Parameter for Swerling Model I. 50
Figure 5.8. Pd vs Gamma Parameter for Swerling Model II. 51
Figure 5.9. Pd vs Gamma Parameter for Swerling Model III. 51

Figure 5.10. Pd vs Gamma Parameter for Swerling Model IV. 52
Figure 5.11. Matched Filter Time Domain Response. 53
Figure 5.12. Matched Filter Frequency Domain Response. 53
Figure 5.13. Compressed echo using analog pulse compression technique. 54
Figure 5.14. Compressed echo using digital pulse compression technique 54
Figure 5.15. Compressed echo using digital pulse compression followed by transversal filter 55
Figure 5.16. Pd vs Reflection Coefficient for Swerling Model I 56
Figure 5.17. Pd vs Reflection Coefficient for Swerling Model II 57
Figure 5.18. Pd vs Reflection Coefficient for Swerling Model III 58
Figure 5.19. Pd vs Reflection Coefficient for Swerling Model IV 58
Figure 5.20. Pd vs Refractivity for Swerling Model I 59
Figure 5.21. Pd vs Refractivity for Swerling Model II 59
Figure 5.22. Pd vs Refractivity for Swerling Model III. 60
Figure 5.23. Pd vs Refractivity for Swerling Model IV. 60

LIST OF ABBREVIATIONS

CFAR	Constant False Alarm Rate
CUT	Cell Under Test
CW	Continuous Wave
FFT	Fast Fourier Transform
IPP	Inter Pulse Period
MMW	Millimeter Wave
MTI	Moving Target Indicator
PDF	Probability Density Function
PRF	Pulse Repetition Frequency
PRI	Pulse Repetition Interval
RCS	Radar Cross Section
SAW	Surface Acoustic Wave
SNR	Signal to Noise Ratio
UHF	Ultra High Frequency
VHF	Very High Frequency

LIST OF SYMBOLS

D	divergence factor
f_D	doppler frequency
f_r	pulse repetition frequency
γ	gamma parameter
G_r	receiving antenna gain
Γ	reflection coefficient of polarization
H	refractivity exponential decay constant
I_0	bessel function
K_0	scaling constant
λ	wavelength of the propagated wave
m	degree of freedom
M	number of reference cell
n_p	number of integrated pulse
n_{fa}	number of false alarm
N_s	refractivity at the surface
ΔN	refractivity linear decay constant
P_{C_n}	cumulative probability of detection during nth frame
P_D	probability of detection
P_{fa}	probability of false alarm
P_t	peak transmitted power
R_u	unambiguous range
σ_{avg}	average cross section of radar
T_i	dwell interval
V_r	radial velocity of the target
V_T	threshold voltage
Z	random variable with gamma probability density function

CHAPTER ONE

INTRODUCTION

1.1. Radar Fundamentals

The word RADAR is an abbreviation for Radio Detection And Ranging. There are so many applications of Radar system both in civil and military sector. Radar can be used to detect aircraft, ships, spacecraft, guided missiles, motor vehicles, weather formations, and terrain.

1.1.1. Definition and basic function

Radar is an electromagnetic system for the detection and location of reflecting objects such as aircraft, ships, spacecraft, vehicles, people and the natural environment. In general, radar systems use modulated waveforms and directive antennas to transmit electromagnetic energy into a specific volume in space to search for targets. Objects (targets) within a search volume will reflect portions of this energy (radar returns or echoes) back to the radar. This small echo signal along with noise is processed by high sensitivity signal processor to determine the exact location, range, velocity, angular position, size and other target identifying information varying according to the type of radar used. The modern uses of radar are highly diverse, including air traffic control, radar astronomy, air-defense systems, antimissile systems, marine radars to locate landmarks and other ships; aircraft anti-collision system, ocean surveillance system, outer space surveillance and rendezvous systems, meteorological precipitation monitoring, altimetry and flight control systems; guided missile target locating systems; and ground-penetrating radar for geological observations. High tech radar systems are associated with digital signal processing and capable of extracting useful information from very high noise levels. There are no competitive techniques that can accurately measure long ranges in both clear and adverse weather as well as can radar. Conventional radars operate using radio waves or microwaves. Radar can also make use of other parts of the electromagnetic spectrum.

The most important functions that radar can perform are

- Resolution
- Detection
- Measurement
- Tracking

Resolution corresponds to radar's ability to resolve (separate) one target signal from another. Larger bandwidths give better resolution in the range parameter, while long transmitted pulses give better resolution in frequency.

Detection function is the ability of the radar to be able to sense the presence of the reflected target signal in the radar receiver. The function is complicated by the unwanted reflected signal (clutter) and the receiver noise.

- Noise is reduced by better receiver design and transmitting signals with larger energy per pulse.
- Clutter is reduced by proper signal design and appropriate signal-processing methods.

Measure function is radar's ability to measure a targets position in 3-D space, its velocity vector, angular direction, and vector angular velocity. Advanced radars even can measure target extent (size), shape, and classification (truck, tank etc.). With the advancement of technology classification of target may become the fourth most important function of radar.

Tracking function enables radar not only to recognize the presence of a target but to determine the target's location in range and in one or two angle coordinates. As it continues to observe a target over time, the radar can provide the target's trajectory, or track and predict where it will be in the future.

1.1.2. Basic RADAR block diagram

A simplified pulsed radar block diagram is illustrated in Figure 1.1. This shows a Radar where the transmitter and the receiver are in same place.

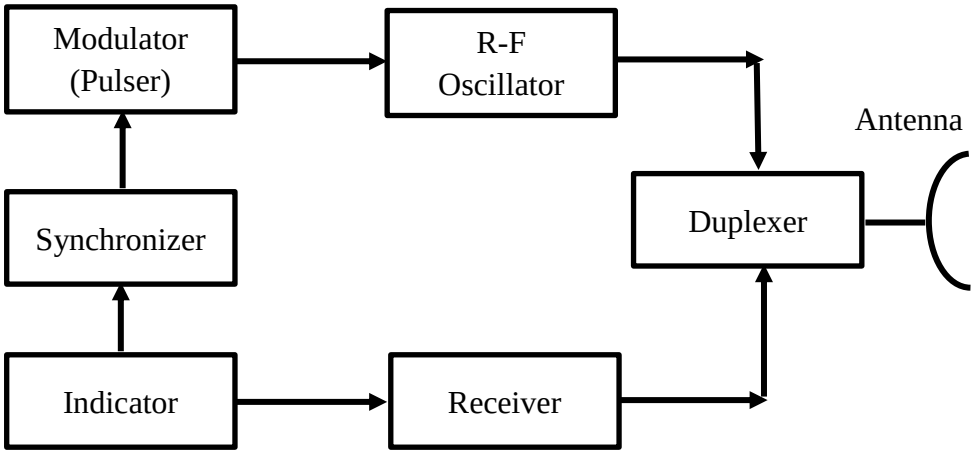

Figure 1.1. Basic Radar Block Diagram.

A modulated signal is generated and sent to the antenna by the modulator/transmitter block. Switching the antenna between the transmitting and receiving modes is controlled by the duplexer. The duplexer allows one antenna to be used to both transmit and receive. During transmission it directs the radar electromagnetic energy towards the antenna. Alternatively, on reception, it directs the received radar echoes to the receiver. The receiver amplifies the radar returns and prepares them for signal processing. Extraction of target information is performed by the signal processor block. The target's range, R, is computed by measuring the time delay Δt; it takes a pulse to travel the two-way path between the radar and the target. Since electromagnetic waves travel at the speed of light, $c = 3 \times 10^8$ m/s, then

$$R = \frac{c\Delta t}{\tau} \tag{1.1}$$

Here, R is in meters and Δt is in seconds.

1.1.3. Background of RADAR

Neither a single nation nor a single person can say that the discovery and development of radar technology was his (or its) own invention. One must see the knowledge about "Radar" than an accumulation of many developments and improvements, in which any scientists from several nations took part in parallel. In the past, there are nevertheless some milestones, with the discovery of important basic knowledge and important inventions:

1865 The Scottish physicist **James Clerk Maxwell** presents his *Theory of the Electromagnetic Field* (description of the electromagnetic waves and their propagation).

It was demonstrated that electric and magnetic fields travel through space in the form of waves, and at the constant speed of light.

1886 The German physicist **Heinrich Rudolf Hertz** discovered electromagnetic waves, thus demonstrating the Maxwell theory.

1897 The Italian inventor **Guglielmo Marconi** achieved the first long distance transmission of electromagnetic waves. In his first experiments he used a wire to wooden pole. In Italian a tent pole is known as *l'antenna centrale* and the pole with a wire alongside it used as an aerial was simply called *l'antenna*. Today Marconi is known as pioneer of radio communication.

1904 The German engineer **Christian Hülsmeyer** invents the "Telemobiloscope" for a traffic monitoring on the water in poor visibility. This is the first practical radar test. Hülsmeyer apply his invention for a patent in Germany, France and the United Kingdom.

1921 The invention of the Magnetron as an efficient transmitting tube by the US-american physicist **Albert Wallace Hull**.

1922 The American electrical engineers **Albert H. Taylor** and **Leo C. Young** of the Naval Research Laboratory (USA) locate a wooden ship for the first time.
1930 Lawrence A. Hyland (also of the Naval Research Laboratory), locates an aircraft for the first time.

1931 A ship is equipped with radar. As antennae are used parabolic dishes with horn radiators.

1936 The development of the Klystron by the technicians **George F. Metcalf** and **William C. Hahn**, both General Electric. This will be an important component in radar units as an amplifier or an oscillator tube.

1939 Two engineers from the university in Birmingham, **John Turton Randall** und **Henry Albert Howard Boot** built a small but powerful radar using a Multicavity-Magnetron. The B–17 airplanes were fitted with this radar. Now they could find and thus combat the German submarines in the night and in fog.

1940 Different radar equipment are developed in the USA, Russia, Germany, France and Japan. The development of the Air Force to major branch of service, the radar technology undergoes a strong development boost during the World War II, and radar sets were used during the "Cold War" in large numbers along the inner German border.

1.1.4. Classification of RADAR

Radar systems have different qualities and technologies. There are many points for radar Classifications.

A. The Separation Between Transmitter and Receiver

a. **Monostatic Radar:** Both transmitter and receiver in the same location.
b. **Bistatic Radar:** The transmitter and receiver in different locations.
c. **Multi-static Radar:** One transmitter and several receivers in different locations.

B. Installation or Location:

a. **Ground based radar:** This type of radar is characterized by:
    i. Very large antenna.
    ii. Great size and weight.
    iii. Long detection range.
    iv. Used as long range surveillance radar.
b. **Naval Radars:** They are used as navigation aids and safety device to locate buoys, shore lines, and other ships.
c. **Airborne Radars:** They are usually used on aircraft so they have as possible as small size and weight, they are used in navigation, terrain following and avoidance, weather warning radar and surface mapping radar.
d. **Space Based Radars:** They may be used to assist in guidance of spacecraft and for remote sensing of the land and sea.

C. Measured Coordinates

a. **One Dimensional (1-D) Radar:** Range finder measures the range.
b. **Two Dimensional (2-D) Radar:** measures both range and azimuth.
c. **Three Dimensional (3-D) Radar:** measures range, azimuth and elevation.

D. Transmission Waveform

a. **Continuous Wave (CW) Radar**: It is based on transmission of CW radio frequency energy. When CW energy is reflected from moving target, the return is Doppler shifted. It is used as speed traps and speed meters.
b. **Frequency Modulated Continuous Wave (FMCW)**: CW radar cannot indicate target range. One way to solve the problem is to modulate the

transmitter output frequency. A triangular or sinusoidal modulating wave form is commonly used by measuring the difference of frequency between the instantaneous transmitter frequency and echo.

c. **Pulsed Radar:** Electromagnetic energy is transmitted as a series of pulses. Target range is found by measuring the time for echoes to return to the receiver. There are several forms of pulse radar such as:

E. Type of Processing:

a. Coherent.
b. MTI and Pulse Doppler.
c. Non-coherent.
d. Phased Array Radar.

1.1.5. Radar frequency bands

The table below has the radar classification based on the operating frequency:

Table 1.1. Frequency Band of RADAR

Letter Designation	***Frequency (GHz)***	***Usage***
HF	0.003~0.03	Over the horizon radar.
VHF	0.03~0.3	Very-long-range surveillance.
UHF	0.3~1.0	Very-long-range surveillance.
L-band	1.0~2.0	Long-range surveillance, Enroute traffic control.
S-band	2.0~4.0	Moderate range surveillance, Terminal air traffic control, Long range weather.
C-band	4.0~8.0	Long range tracking, Airborne weather detection.
X-band	8.0~12.5	Airborne intercept & weather radar, Short range tracking, Missile guidance, Mapping marine radar.
Ku-band	12.5~18.0	High resolution mapping, satellite altimetry.
K-band	18.0~26.5	Little Used (water vapor).
Ka-band	26.5~40.0	Very high resolution mapping, Short range tracking, Airport surveillance.
V, W	40.0~110.0	Smart munitions, remote sensing
MMW	110.0+	Experimental, remote sensing.

1.2. Continuous Wave and Pulsed Radars

Continuous wave radar systems are those which use a stable frequency continuous wave for transmission and reception.

1.2.1. Continuous wave RADAR

CW radars depend on the doppler frequency shift of the echo signal, caused by a moving target, to separate in the frequency domain the weak echo signal from the large transmitted signal and the echoes from fixed clutter (land, sea or weather), as well as to measure the radial velocity of the target. This doppler shift is related to the target velocity by the relation:

$$f_D = \frac{2V_r}{\lambda} \tag{1.2}$$

The main advantages of the CW radars are:

a. Simple to manufacture.
b. No minimum or maximum range (broadcast power level imposes a practical limit on range).
c. Maximize power on a target due to continuous broadcasting.

However, they also have the following disadvantages:

a. They can only detect moving targets, as stationary targets (along the line of sight) will not cause a Doppler shift.
b. They cannot measure range. Range is normally measured by timing the delay between a pulse being sent and received, but as CW radars are always broadcasting, there is no delay to measure. Ranging can be implemented, however, by use of a technique known as frequency modulated continuous-wave radar.

1.2.2. Pulsed RADAR

Pulsed Radars use a train of pulsed waveforms with modulation. Basing on pulse repetition frequency or PRF (definition given in the next section), Pulsed radars are classified as low PRF, medium PRF and High PRF. Low PRF radars are used primarily for ranging where target velocity is not needed. High PRF radars are used for measuring target velocity (Doppler Shift).

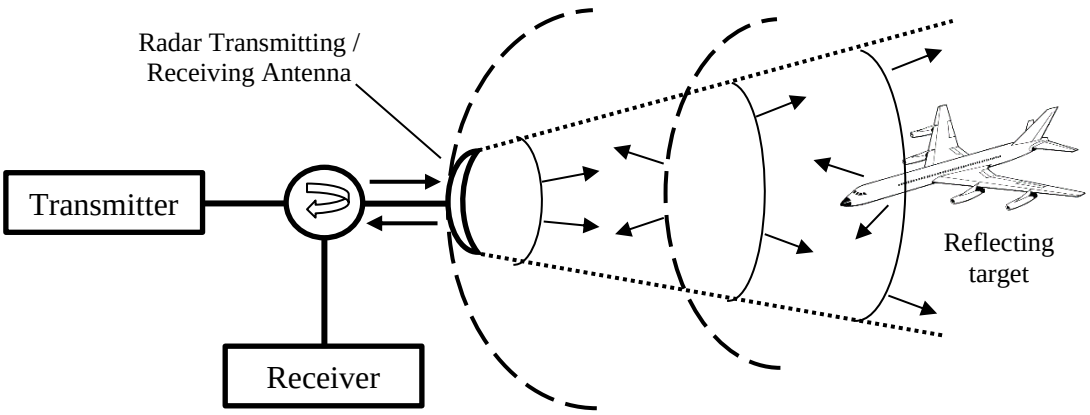

Figure 1.2. Transmitter and Receiver of Radar.

One of pulse radar advantages is that the transmitter is turned off most of the time. The receiver can listen for returning echoes without any interference from the transmitter. Pulsed radars which extract the doppler frequency shift are called either moving target indication (MTI) or pulse doppler radars depending on their particular values of pulse repetition frequency and duty cycle. MTI radar has a low PRF and a low duty cycle. A pulse doppler radar on the other hand has a high PRF and a high duty cycle.

1.3. Radar Terminologies

There are some terminologies which are used to describe different equations and phenomenon in RADAR system.

1.3.1. Pulse repetition frequency

Pulsed radar uses a train of pulse for transmission and reception as illustrated Figure 1.2. The time interval between any two transmitted pulses is known as the Pulse Repetition Interval (PRI) or Inter Pulse Period (IPP) denoted by T. The inverse of PRI is called Pulse Repetition Frequency (PRF) denoted by f_r. During each PRI radar radiates energy only for τ (pulse width) seconds and listens for target returns for rest of the PRI.

Here

$$f_r = \frac{1}{PRI} = \frac{1}{T} \tag{1.3}$$

Radar transmitting duty cycle is

$$d_t = \frac{\tau}{T} \tag{1.4}$$

And the radar average transmitted power is

$$P_{avg} = P_t * d_t \tag{1.5}$$

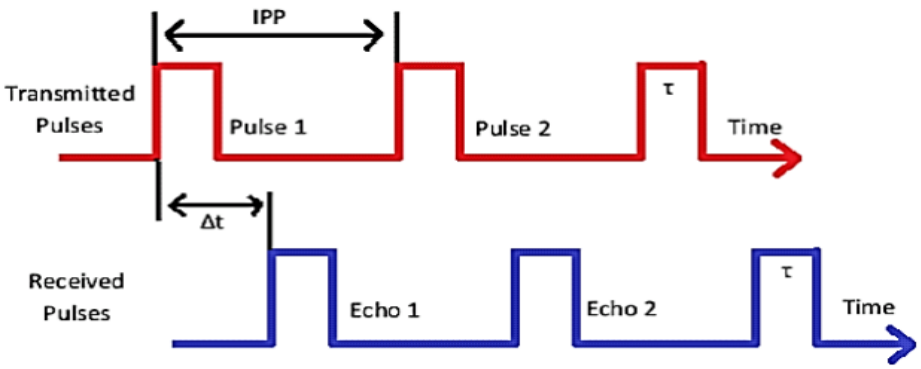

Figure 1.3. PRF and IPP.

From the above equations it is seen that increasing the pulse width means increasing the transmitting duty cycle which in turn increases the radar average transmitted power thereby increasing the SNR.

1.3.2. Maximum unambiguous range

Once a pulse is transmitted sufficient time must elapse to allow all echo signals to return to the radar before the next pulse is transmitted. The rate at which pulses maybe transmitted, therefore, is determined by the longest range at which targets are expected. If the time between pulses T_p is too short an echo signal from a long-range target might arrive after the transmission of the next pulse and be mistakenly associated with that pulse rather than the actual pulse transmitted earlier. This can result in an incorrect or ambiguous measurement of the range. The range beyond which targets appear as second-time around echoes is the maximum unambiguous range, R_u and is given by

$$R_u = \frac{cT}{2} \tag{1.6}$$

Where T_p = pulse repetition period = $1/f_p$ and f_p = pulse repetition frequency (prf). Therefore, the maximum unambiguous range (R_u) corresponds to half of PRI.

1.3.3. Range resolution

It is the radar`s ability to detect targets in close proximity to each other as distinct objects. Radars have a minimum range R_{min} and a maximum range R_{max}. The whole range area is divided into number of range bins or gates (M) each of width ΔR. Targets separated by at least ΔR can be completely resolved in range. Targets within the same range bin can be resolved in cross range (horizontally) utilizing signal processing techniques. To find the minimum ΔR let us assume two targets separated by $\frac{c\tau}{4}$ as shown in Figure 1.4.

In this case, when the pulse trailing edge strikes target 2 the leading-edge would have traveled backwards a distance $c\tau$ and the returned pulse would be composed of returns from both targets.

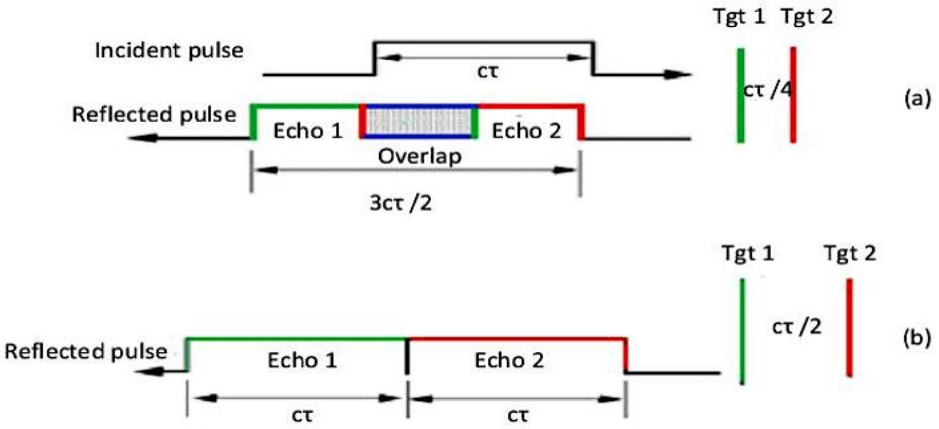

Figure 1.4. Range resolutions (a) Two unresolved targets, (b) Two resolved targets.

However, if the two targets are at least cτ/2 apart, then as the pulse trailing edge strikes the first target the leading edge will start to return from target 2, and two distinct returned pulses will be produced, as illustrated by Figure 1.5. Thus, ΔR should be greater or equal to $c\tau/2$. And since the radar bandwidth B is equal to 1/τ, then

$$\Delta R = \frac{c\tau}{2} = \frac{c}{2B} \tag{1.7}$$

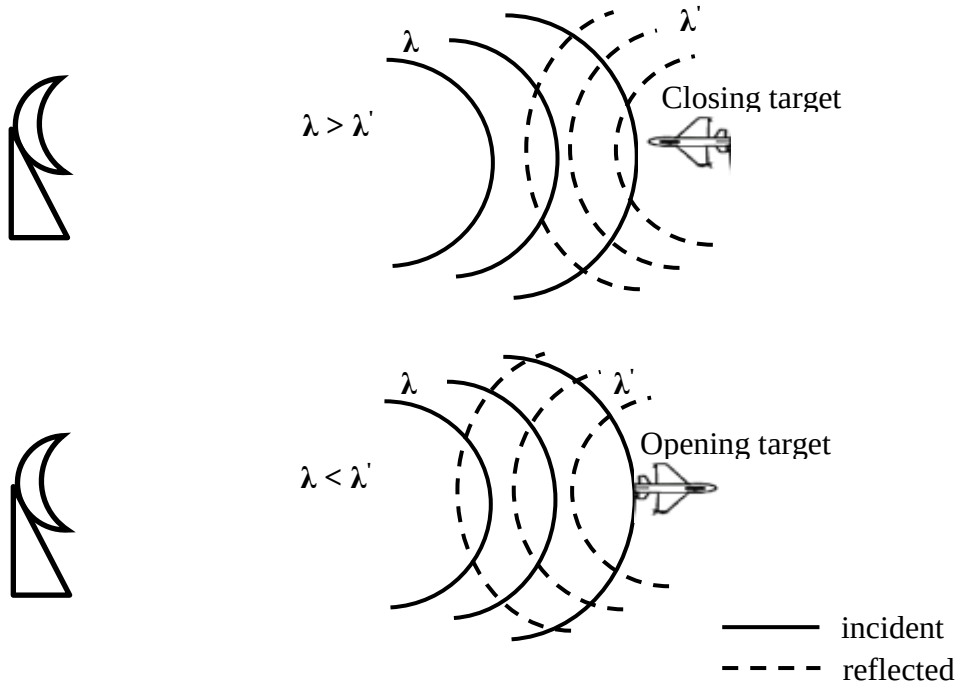

Figure 1.5. Effect of target motion on the reflected equi-phase waveforms.

In general, radar designers seek to minimize in order to enhance the radar performance. As suggested by Eq. 1.5, in order to achieve fine range resolution one must minimize the pulse width. However, this will reduce the average transmitted power and increase the operating bandwidth. Achieving fine range resolution while maintaining adequate average transmitted power can be accomplished by using pulse compression techniques.

Figure 1.5 explains the effect of target motion on the reflected equi-phase waveforms. For opening target and closing target the wavelength and frequencies are not similar.

1.3.4. Doppler shift

Doppler shift is an apparent change in frequency (or wavelength) due to the relative motion of two objects. When the two objects are approaching each other, the doppler shift causes a shortening of wavelength or increase in frequency. When the two objects are moving away from each other, the doppler shift causes a lengthening of wavelength or decrease in frequency.

To measure speed, an accurate sample of the original phase of the transmitted signal must be maintained for comparison against the reflected signal for a doppler radar system.

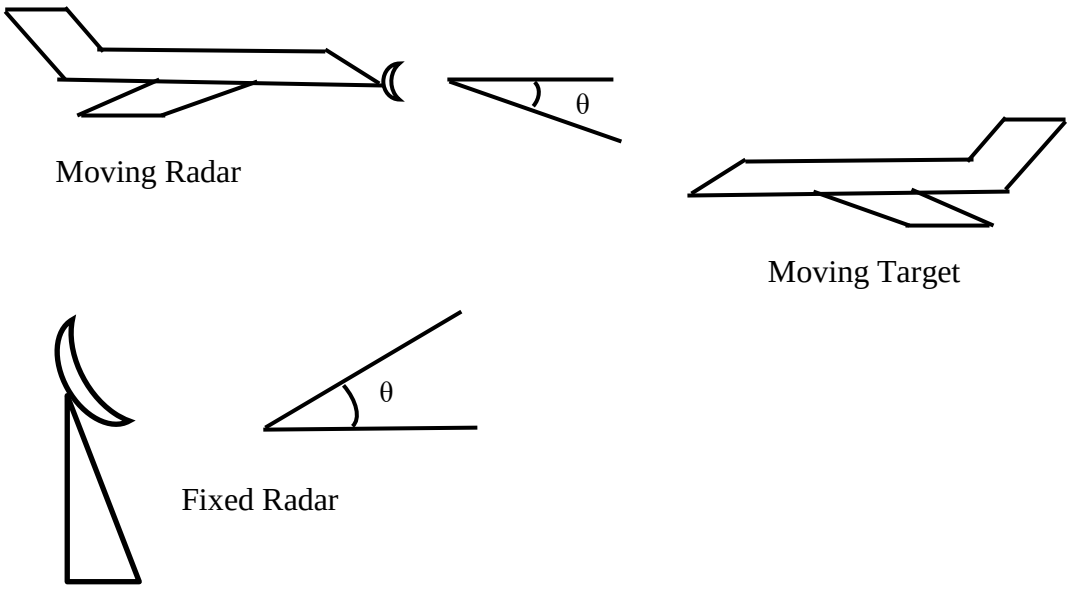

Figure 1.6. Doppler shift due to moving radar and targets

Angle shown (θ) is for elevation differences only; if there is also an azimuthal angle, it must be factored into the equation as $\cos(\alpha)$, where α is the azimuth angle relative to the radar antenna bore sight direction. For fixed radar with moving target:

$$f_D = 2V_T cos\theta \ \frac{f_T}{c} \tag{1.8a}$$

For moving radar with moving target:

$$f_D = 2(V_R + V_T) cos\theta \ \frac{f_T}{c} \tag{1.8b}$$

Where f_D = doppler frequency, f_T = transmitted frequency, V_T = target velocity

V_R = radar velocity, c = speed of light.

1.3.5. Coherence

A Radar is coherent if there is continuity in phase from one transmitted pulse to another. It is radar's ability to maintain an integer multiple of wavelengths between the equiphase wave fronts of any two successive pulses. Coherence is a requirement to measure (extract) the received signal phase. Since Doppler represents a frequency shift in the received signal, then only coherent or coherent-on-receive radars can extract Doppler information. This is because the instantaneous frequency of a signal is proportional to the time derivative of the signal phase. More precisely if f_i is the instantaneous frequency and $\varphi(t)$ is the signal phase.

$$f_i = \frac{1}{2\pi}\frac{d\varphi(t)}{dt} \tag{1.9}$$

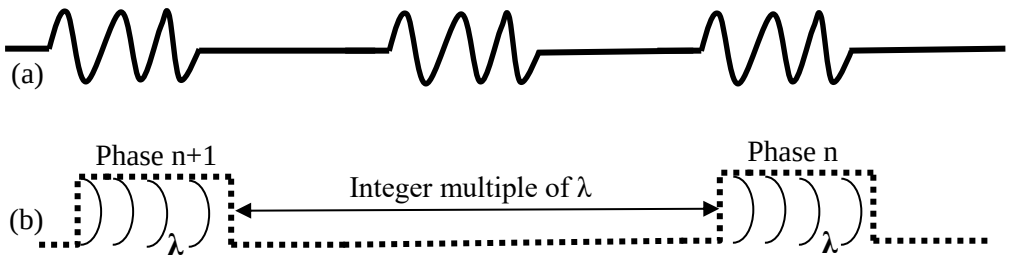

Figure 1.7. (a) Phase continuity between consecutive pulses (b) Maintaining an integer multiple of wavelengths between the equi-phase wave fronts of any two successive pulses guarantees coherency.

CHAPTER TWO

BRIEF OVERVIEW ON DETECTION CAPABILITY

2.1. Introduction

Fundamental concepts of Radar system and different terminologies related to this thesis are discussed in the previous chapter. Objective of the research, organization of the chapters and literature review on detection capability of various target models are discussed in this chapter.

2.2. Objective of the Thesis

The main objective of this thesis is to analyze the target models and improve detection capability with different methods. The main purposes of the thesis are:

a. To analyze of different target models of Swerling where the targets are not fixed to find out better accuracy.
b. To use different false alarm rate to identify the optimal value for reducing SNR (dB) loss.
c. To develop a relationship between probability of detection (P_d) and constant false alarm rate (CFAR).
d. To determine the optimal value of CFAR from P_d vs CFAR relationship.
e. To build up a system model with improved detection capability from the optimal value of CFAR.
f. To show a comparative statistic of P_d vs SNR relationship for different values of integrated pulse.
g. To reduce Side lobes Using Transversal Filter with Digital Pulse Compression Technique to improve detection capability of radar.
h. To improve detection capability of radar system in different conditions of earth atmosphere.

2.3. Organization of the Thesis

Chapter 1 is an introductory chapter. It contains the origin and fundamentals of radar system. Different types of Radar and its terminologies are

discussed in this chapter.

Chapter 2 depicts the objective, organization of the thesis and literature review. Similar researches are studied and compared on respective field.

Chapter 3 explains the methodology in detail and the key issues in implementation. Analysis of target models and their various behaviors with different parameters are discussed here.

Chapter 4 explains how the limits of the methodology are scientifically assessed. Simulation is done to evaluate the system performance of Radar system.

Chapter 5 provides graphical representation of simulation. Observation from the simulation drives towards the result to improve detection capability in Radar system. Observed results from different techniques are compared and discussed in this chapter.

Chapter 6 demonstrate the concluding remarks of the research work. Future research works are also proposed here based on this thesis.

2.4. Literature Review

The related work can be described as: (i) analysis of RADAR Performance for Different fluctuating target models of various false alarm rate (ii) finding out the probability of detection capability and CFAR loss under fluctuating targets of different Swerling model for various gamma parameters in radar (iii) analysis the performance of radar in case of atmospheric attenuation of different layers of earth atmosphere for various target models (iv) reduction of side lobes using transversal filter with digital pulse compression technique to improve detection capability of radar.

2.4.1. Detection capability and false alarm rate

A significant number of researches have been carried out to find out the detection capability of fluctuating targets for Swerling models under various false alarm rate. Xiangguang Leng, Kefeng Ji, Kai Yang and Huanxin Zou developed a CFAR algorithm for target detection in synthetic aperture Radar [1]. Authors used the algorithm for the case of ship detection. G. Gigli and G. A. Lampropoulos showed CFAR gamma detector in their research [2]. In [15], the authors propose a theoretical simulation based model in which probability of detection of radar signal in terms of signal to noise ratio (SNR) was

shown for single pulse. In this case, the two new fluctuation models, designated as expanded category 2A and 2B generalized Swerling models have been discussed which provide increased flexibility to produce a better match with actual target fluctuations. Original Swerling I model often produces probability of detection that are unrealistically low at high SNR values. They proposed the new models which can be used to produce more reasonable results in such cases.

Thomas Backes and L. Donnie Smith improved the Radar Cross Section (RCS) model for censored Swerling III and IV target models in their paper [16]. They showed a relationship between error (dB) and average RCS. For different number of samples simulation has been completed there. It is proved that the censored maximum likelihood estimate has improved the performance over the uncensored system. The increased performance is observed at low level of Radar Cross Section. X. Wang, M. Yang, S. Zhu, and Y. Lin show regionlets for generic object detection [23]. A. De Maio, A. Farina, and G. Foglia discussed about target fluctuation models and their application to radar performance prediction [29].

Mohamed B. El Mashade found out the probability of detection for fluctuating targets for different values of SNR in his paper [20]. He used adaptive detection to evaluate the performance of RADAR under various Swerling Model. Matched filter, quadratic rectifier, non-coherent integration were used to implement in his technique. To show a complete set of performance curves the analytical results were used there. The result of this paper resembles detection capability in homogeneous and various target situations and the change of false alarm rate with the strength of interfering targets. The author showed the estimation set and the required signal to noise ratio to get a predetermined operating point of fixed levels for detection and false alarm rates.

Wentao An, Chunhua Xie, and Xinzhe Yuan developed an improved iterative censoring scheme for CFAR ship detection with SAR imagery [5]. M. B. El Mashade analyzed the performance evaluation of adaptive detection [6]. The author considered fluctuating radar targets in his research.

2.4.2. Probability of detection and CFAR loss in terms of threshold voltage

George Gigli and George A. Lampropoulos tried to find a new gamma CFAR detector in their research [2]. They show a relationship between probability of detection and SNR

for generalized gamma parameter. Gamma Function is directly related to the threshold voltage of the RADAR received signal. New model of probability density function (PDF) was also introduced in their research. A relationship was developed between modeled PDF and clutter PDF through the parametric generalized gamma estimation. A. Aubry, A. De Maio, Bo Jiang, and Shuzhong Zhang found the ambiguity function shaping for cognitive radar via complex quartic optimization [4].

In [10], L. Kong, G. Cui, X. Yang, W. Yi, and B. Wang predicted the performance of Constant False Alarm Rate (CFAR) for non-independent and non-identically distributed gamma fluctuating targets. They simulated the result for Cell Averaging CFAR and Ordered Statistic CFAR to detection the probability. The theoretical result of Probability of detection and SNR has been compared with Monte Carlo Simulation. The detection performance was evaluated via Numerical expression. The theoretical result found in their research is precisely consistent with Monte Carlo Simulation.

David A. Shnidman shows analytical characteristics of expanded Swerling Model [6]. The relationship between detection capability and SNR was developed for average single pulse. He explained that original model of Swerling sometimes produces probability of detection which are unrealistic. He proposed two expanded generalized category model named as 2A and 2B. These models provide better performance in presence of fluctuating target. It was observed that the log-normal and Weibull fluctuation models can be used to obtain the suitable Probability of Detection. But those functions are not suitable to evaluate incoherent integration. R. Mamgain, R. Jain, D. Deb, and D. Seshagiri develop the two level CFAR algorithm for multiple target detection [33].

F. D. A. Garcia, A. C. F. Rodriguez, G. Fraidenraich, and J. C. S. Santos Filho analyzed CA-CFAR detection performance in homogeneous Weibull clutter [7]. Y. Wang, W. Xia, and Z. He show the CFAR knowledge-aided radar detection With Heterogeneous Samples [8]. C. H. Gierull finds the demystifying capability of sublook correlation techniques for vessel detection in SAR imagery [11]. E. Chaumette, U. Nickel, and P. Larzabal detection and parameter estimation of extended targets using the generalized monopulse estimator [12]. Y. Cui, G. Zhou, J. Yang, and Y. Yamaguchi represent the iterative censoring for target detection in SAR images in their research [19].

2.4.3. Reduction of side lobes using pulse compression technique

Tortoli, Guidi, and Atzeni discussed about the pulse compression technique in their research paper [13]. They showed comparison in digital filter & matched filter for the implementation of compression technique. Ideal and experimental compressed pulses have been compared for various bandwidth. From the research it is observed that the digital compressed pulse shows an almost ideal behavior. In this case sidelobe levels slightly deviate at around -60 dB. FFT processor was used there. Surface Acoustic Wave (SAW) can be used to design filter according to the same criteria used in the digital technique. Yu Gen-miao, Wu Shun-jun, and Luo Yong-jian show the doppler properties of polyphase pulse compression codes under different side-lobe reduction techniques [14].

2.4.4. Atmospheric attenuation of Radar signal

Few researchers have done their researches in the field of atmospheric attenuation and losses occur from it in Radar system. In general, there are some models regarding atmospheric radio refractive index. R. Du, F. Norouzian, E. Marchetti, B. Willetts, M. Gashinova, and M. Cherniakov show the characterization of attenuation by sand in low-terahertz band [9]. Smith and Weintraub [30] present the relationship of refraction at any particular altitude as a function of atmospheric constituents and their respective partial pressure and temperature which is very important for determining the detection capability.

Bean and Thayer [18] offer a model of how refractivity changes with altitude. In their model, nature of refractivity is such that on the average it has a fairly linear height gradient to about 1 km above ground, then decays exponentially beyond that. Below an altitude of 9 km, the refractivity depends on surface conditions, which varies with region, season, time of day, etc. Above 9 km, the refractivity is relatively surface-condition independent. J. Branson, S. Wooding, and W. N. Dawber discuss about modelling of the littoral environment for real-time radar performance assessment [17].

Surface refractivity varies regionally, and with season and time of day. Various publications by Bean [31], Bean and Dutten [22] and Bean et al. [3] show that refractivity of surface varies from less than 250 during dry months to around 400 along the coast in the month of summer. An average value for number of units is given by Bean as 313. Altshuler [13] reports that his data shows that the average refractivity of global surface

is 324.8 N-units and that the standard deviation of [his] sample is 30.1 N-units. S. L. Durden relates GPM Radar reflectivity profile characteristics to path-integrated attenuation [24]. A. Linkova and G. Khlopov worked with rain intensity. Retrieval of rain intensity by three-frequency radar sensing is discussed in their research [25].

2.5. Conclusion

Related works on similar fields in the case of target detection is discussed in this chapter. Contributions of many researchers are compared with each other which leads to significant decision in this thesis. Objectives of the research are also mentioned here. Target models need to be analyzed for improving detection capability which is shown in next chapter.

CHAPTER THREE

ANALYSIS OF TARGET MODELS

3.1. Introduction

The proposed system of this thesis work consists of four different portions – detection capability of RADAR in presence of False Alarm Rate, findings probability of detection and CFAR loss in terms of threshold voltage, reduction of side lobes using pulse compression technique and atmospheric attenuation of propagated radar wave. RADAR detection capability can be changed due to so many factors. In order to maintain a standard probability of detection some parameters should be kept in optimal range. When false signal is received in the receiver of radar it can affect the threshold voltage. As a result, changes occur in detection capability. In order to avail better performance, Constant False Alarm Rate (CFAR) technique is used. Probability of detection also changes because of CFAR loss. Radar performance also depends on the characteristics of the radar antenna. There are so many side lobes observed in radiation pattern of radar antenna. Suppression of side lobes gives better target detection with main lobe. Behavior of atmosphere is an important phenomenon in transmission of different types of radio waves. Natural component of earth atmosphere may also influence the normal propagation of radar wave. As a result, received signal can be changed from its original value which indicates a false detection of propagated wave.

3.2. Signal Detection in Presence of Noise

Detection of RADAR signal in presence of noise is different from the detection without noise. The input signal to the receiver is composed of the radar echo signal $s(t)$ and additive zero mean white Gaussian noise $n(t)$, with variance Ψ^2. A simplified block diagram of a radar receiver that employs an envelope detector followed by a threshold decision is shown in Figure 3.1. The input noise is assumed to be spatially incoherent and uncorrelated with the signal. The output of the band pass IF filter is the signal $v(t)$, which can be written as [21]

$$v(t) = v_I(t)cos\omega_0 t + v_Q(t)sin\omega_0(t) \qquad (3.1)$$

$$= r(t)\cos\left(\omega_0 t - \phi(t)\right)$$

$$v_I(t) = r(t)cos\varphi(t)$$

$$v_Q(t) = r(t)sin\phi(t)$$

Where $\omega_0 = 2\pi f_0$ is the radar operating frequency, $r(t)$ is the envelope of the $v(t)$, the phase is $\phi(t) = \text{atan}(v_Q/v_I)$, and the subscripts I, Q refer to the in phase and quadrature components respectively.

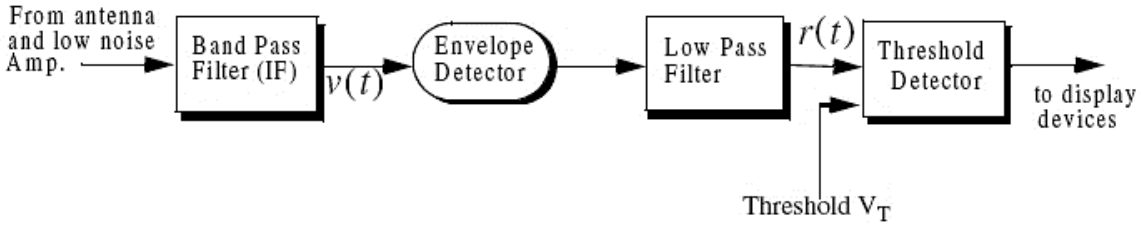

Figure 3.1. Simplified block diagram of an envelope detector and threshold receiver.

A target is detected when $r(t)$ exceeds the threshold value V_T, where we can write,

$$s(t) + n(t) > V_T \quad \text{for Detection}$$

$$n(t) > V_T \qquad \text{False Alarm}$$

When the noise subtracts from the signal (while a target is present) to make $r(t)$ smaller than the threshold is called a miss target. Radar designers try to maximize the probability of detection for a given probability of false alarm. The IF filter output is a complex random variable that is composed of either noise alone or noise plus target return signal (sine wave of amplitude A). The quadrature components are [21]

$$v_I(t) = n_I(t) \tag{3.2a}$$

$$v_Q(t) = n_Q(t) \tag{3.2b}$$

and for the second case,

$$v_I(t) = A + n_I(t) = r(t)cos\varphi(t)$$

$$n_I(t) = r(t)cos\varphi(t) - A$$

$$v_Q(t) = n_Q(t) = r(t)sin\varphi(t) \tag{3.3}$$

Where the noise quadrature components $n_I(t)$ and $n_Q(t)$ are uncorrelated zero mean low pass Gaussian noise with equal variances, Ψ^2. The joint Probability Density Function (pdf) of the two random variables n_I, n_Q is [7]

$$f\left(n_I, n_Q\right) = \frac{1}{2\pi\psi^2}\exp\left(-\frac{n_I^2+n_Q^2}{2\psi^2}\right) \tag{3.4}$$

$$= \frac{1}{2\pi\psi^2} \exp\left(-\frac{(r\cos\varphi - A)^2 + (r\sin\varphi)^2}{2\psi^2}\right)$$

The pdfs of the random variables $r(t)$ and $\phi(t)$, respectively, represent the modulus and phase of $v(t)$. The joint pdf for the two random variables $r(t), \varphi(t)$ is given by [8]

$$f(r, \varphi) = f(n_I, n_Q)|J| \tag{3.5}$$

Where [J] is a matrix of derivatives defined by

$$[J] = \begin{bmatrix} \frac{\partial n_I}{\partial r} & \frac{\partial n_1}{\partial \varphi} \\ \frac{\partial n_Q}{\partial r} & \frac{\partial n_Q}{\partial \varphi} \end{bmatrix} = \begin{bmatrix} cos\varphi & -rsin\varphi \\ sin\varphi & rcos\varphi \end{bmatrix} \tag{3.6}$$

The determinant of the matrix of derivatives is called the Jacobian, and in this case it is equal to

$$|J| = r(t) \tag{3.7}$$

Substituting Eqs. (3.4) and (3.7) into Eq. (3.5) and collecting terms yield [21]

$$f(r, \varphi) = \frac{r}{2\pi\Psi^2} \exp\left(-\frac{r^2 + A^2}{2\Psi^2}\right) \exp\left(\frac{rA\cos\varphi}{\Psi^2}\right) \tag{3.8}$$

The pdf for r alone is obtained by integrating Eq. (3.8) over φ

$$f(r) = \int_0^{2\pi} f(r, \varphi) d\varphi = \frac{r}{\psi^2} \exp\left(-\frac{r^2 + A^2}{2\psi^2}\right) \frac{1}{2\pi} \int_0^{2\pi} \exp\left(\frac{rA\cos\varphi}{\psi^2}\right) d\varphi \tag{3.9}$$

Where the integral inside Eq. (3.9) is known as the modified Bessel function of zero order,

$$I_0(\beta) = \frac{1}{2\pi} \int_0^{2\pi} e^{\beta\cos\theta} d\theta \tag{3.10}$$

As a result,

$$f(r) = \frac{r}{\psi^2} I_0\left(\frac{rA}{\psi^2}\right) \exp\left(-\frac{r^2 + A^2}{2\psi^2}\right) \tag{3.11}$$

Which is the Rice probability density function. If $\frac{A}{\psi^2} = 0$ (noise alone), then Eq. (3.11) becomes the Rayleigh probability density function

$$f(r) = \frac{r}{\psi^2} \exp\left(-\frac{r^2}{2\psi^2}\right) \tag{3.12}$$

Also, when (A/ψ^2) is very large, Eq. (3.11) becomes a Gaussian probability density function of mean A and variance ψ^2:

$$f(r) = \frac{1}{\sqrt{2\pi\psi^2}} \exp\left(-\frac{(r - A)^2}{2\psi^2}\right) \tag{3.13}$$

The density function for the random variable φ is obtained from

$$f(\varphi) = \int_0^r f(r, \varphi) dr \tag{3.14}$$

3.3. Probability of False Alarm

The probability of false alarm P_{fa} is defined as the probability that a sample R of the signal $r(t)$ will exceed the threshold voltage V_T when noise alone is present in the radar,

$$P_{fa} = \int_{V_T}^{\infty} \frac{r}{\Psi^2} exp\left(-\frac{r^2}{2\Psi^2}\right) dr = \exp(-\frac{V_T^2}{2\Psi^2}) \tag{3.15a}$$

$$V_T = \sqrt{2\Psi^2 \ln\left(\frac{1}{P_{fa}}\right)} \tag{3.15b}$$

Figure 3.2 shows a plot of the normalized threshold versus the probability of false alarm. From the figure it is evident that P_{fa} is very sensitive to small changes in the threshold value.

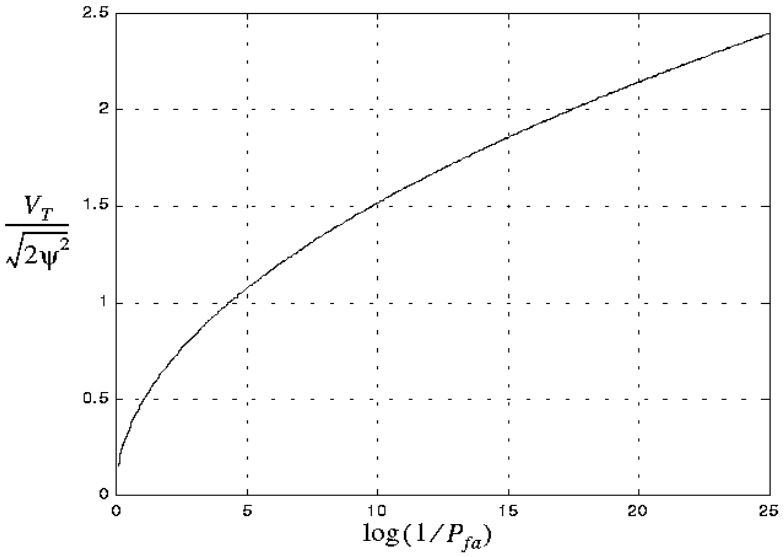

Figure 3.2. Normalized detection threshold versus probability of false alarm.

The false alarm time T_{fa} is related to the probability of false alarm by

$$T_{fa} = \frac{t_{int}}{P_{fa}} \tag{3.16}$$

Where t_{int} represents the radar integration time, or the average time that the output of the envelope detector will pass the threshold voltage. Since the radar operating bandwidth B is the inverse of t_{int}, then by substituting Eq. (3.15) into Eq. (3.16) we can write T_{fa} as

$$T_{fa} = \frac{1}{B}\exp(\frac{V_T^2}{2\psi^2}) \tag{3.17}$$

Minimizing T_{fa}means increasing the threshold value, and as a result the radar maximum detection range is decreased. Therefore, the choice of an acceptable value for T_{fa} becomes a compromise depending on the radar mode of operation. The false alarm

number n_{fa} was defined by Marcum as the reciprocal of P_{fa}. Using Marcum's definition of the false alarm number, the probability of false alarm is given by $P_{fa} \approx \ln(2)(n_p/n_{fa})$, where $n_p > 1$ is the number of pulses and $P_{fa} < 0.007$.

3.4. Probability of Detection

The probability of detection P_d is the probability that a sample R of $r(t)$ will exceed the threshold voltage in the case of noise plus signal [21],

$$P_D = \int_{V_T}^{\infty} \frac{r}{\Psi^2} I_o(\frac{rA}{\Psi^2}) \exp[-(r^2 + A^2)/2\Psi^2] dr \tag{3.18}$$

Where r is the envelope of the threshold voltage, A is the amplitude of the return signal with variance of noise Ψ^2. If we assume that the radar signal is a sine waveform with amplitude A, then its power is $A^2/2$.

Now, by using $SNR = A^2/2\Psi^2$ (single-pulse SNR) and $(V_T^2/2\psi^2) = \ln(1/P_{fa})$, then Eq. (3.18) can be rewritten as

$$P_D = \int_{2\psi^2 \ln(1/P_{fa})}^{\infty} \frac{r}{\Psi^2} I_0(\frac{rA}{\Psi^2}) \exp\left(-\frac{r^2+A^2}{2\Psi^2}\right) dr = Q\left[\sqrt{\frac{A^2}{\psi^2}}, \sqrt{2\ln\left(\frac{1}{P_{fa}}\right)}\right] \tag{3.19}$$

$$Q[\alpha, \beta] = \int_{\beta}^{\infty} \zeta I_0(\alpha\zeta) e^{-(\zeta^2+\alpha^2)2} d\zeta \tag{3.20}$$

Q is called Marcum's Q-function. When P_{fa} is small and P_D is relatively large so that the threshold is also large, Eq. (3.20) can be approximated by

$$P_D \approx F\left(\frac{A}{\Psi} - \sqrt{2\ln\left(\frac{1}{P_{fa}}\right)}\right) \tag{3.21}$$

3.5. Pulse Integration

When a target is illuminated by the radar beam it normally reflects numerous pulses. The radar probability of detection is normally enhanced by summing all (or most) of the returned pulses. The process of adding radar echoes from many pulses is called radar pulse integration. Pulse integration can be performed on the quadrature components prior to the envelope detector. This is called coherent integration or pre-detection integration. Coherent integration preserves the phase relationship between the received pulses, thus a moderate signal amplitude is achieved. Alternatively, pulse integration performed after the envelope detector (where the phase relation is destroyed) is called non-coherent or post-detection integration.

3.5.1. Coherent integration

In coherent integration, if a perfect integrator is used (maximum efficiency), then integrating n_p pulses would improve the SNR by the same factor. Otherwise, integration loss occurs which is always the case for non-coherent integration. In order to demonstrate this signal buildup, consider the case where the radar return signal contains both signals plus additive noise. The mth pulse is

$$y_m(t) = s(t) + n_m(t) \tag{3.22}$$

where $s(t)$ is the radar return of interest and $n_m(t)$ is white uncorrelated additive noise signal. Coherent integration of n_p pulses yields [21]

$$z(t) = \frac{1}{n_p}\sum_{m=1}^{n_p} y_m(t) = \sum_{m=1}^{n_p}\frac{1}{n_p}[s(t) + n_m(t)] = s(t)\sum_{m=1}^{n_p}\frac{1}{n_p}n_m(t) \tag{3.23}$$

The total noise power in $z(t)$ is equal to the variance. More precisely,

$$\psi_{nz}^2 = E\left[\left(\sum_{m=1}^{n_p}\frac{1}{n_p}n_m(t)\right)\left(\sum_{l=1}^{n_p}\frac{1}{n_p}n_l(t)\right)^*\right] \tag{3.24}$$

where $E[\,]$ is the expected value operator. It follows that [21]

$$\psi_{nz}^2 = \frac{1}{n_p^2}\sum_{m,l=1}^{n_p} E[n_m(t)n_l^*(t)] = \frac{1}{n_p^2}\sum_{m,l=1}^{n_p}\Psi_{ny}^2\delta_{ml} = \frac{1}{n_p}\psi_{ny}^2 \tag{3.25}$$

Where ψ_{ny}^2 is the single pulse noise power and δ_{ml} is equal to zero for $m \neq l$ and unity for $m = l$. Observation of Eqs. (3.23) and (3.25) shows that the desired signal power after coherent integration is unchanged, while the noise power is reduced by the factor $1/n_p$. Thus, the SNR after coherent integration is improved by n_p.

We may denote the single pulse SNR required to produce a given probability of detection as $(SNR)_1$. Also, denote $(SNR)_{n_p}$ as the SNR required to produce the same probability of detection when n_p pulses are integrated. It follows that

$$(SNR)_{n_p} = \frac{1}{n_p}(SNR)_1 \tag{3.26}$$

The requirements of remembering the phase of each transmitted pulse as well as maintaining coherency during propagation is very costly and challenging to achieve. In practice, most radar systems utilize non-coherent integration.

3.5.2. Non-Coherent Integration

Non-coherent integration is often implemented after the envelope detector, also known as the quadratic detector. A block diagram of radar receiver utilizing a square law detector and non-coherent integration is illustrated in Figure 3.3. In practice, the square

law detector is normally used as an approximation to the optimum receiver. The *pdf* for the signal $r(t)$ was derived earlier and it is given in Eq. (3.11). We can define a new dimensionless variable y as

$$y_n = \frac{r_n}{\Psi} \tag{3.27}$$

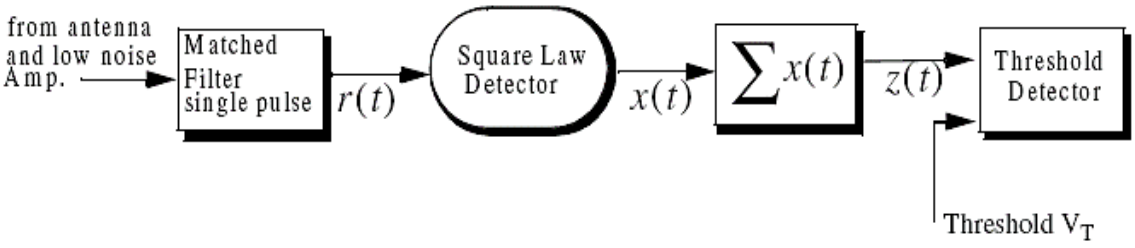

Figure 3.3. Block diagram of a square law detector and non-coherent integration.

3.6. Detection of Fluctuating Targets

The discussion about the probability of detection so far, we assumed a constant target cross section (non-fluctuating target). However, when target scintillation is present, the probability of detection decreases, or equivalently the SNR is reduced

3.6.1. Detection of probability density function

The probability density functions for fluctuating targets can be written as for Swerling I and II type targets [21]

$$f(A) = \frac{1}{A_{av}} \exp\left(-\frac{A}{A_{av}}\right) \qquad A \geq 0 \tag{3.28}$$

For Swerling III and Swerling IV targets, it can be expressed as,

$$f(A) = \frac{4A}{A^2_{av}} \exp\left(-\frac{2A}{A_{av}}\right) \qquad A \geq 0 \tag{3.29}$$

where A_{av} denotes the average RCS over all target fluctuations.

The probability of detection for a scintillating target is computed in a similar fashion to Eq. (3.18), except in this case $f(r)$ is replaced by the conditional *pdf* $f(r/A)$. Performing the analysis for the general case

$$f\left(\frac{z}{A}\right) = \left(\frac{2z}{\frac{npA^2}{\Psi^2}}\right)^{\frac{n_p-1}{2}} \exp\left(-z - \frac{\frac{1}{2}n_pA^2}{\psi^2}\right) I_{n_p} - 1\left(\sqrt{2n_pz\left(\frac{A^2}{\Psi^2}\right)}\right) \tag{3.30}$$

Where

$$f(z) = \int f\left(\frac{z}{A}\right) f(A) dA \tag{3.31}$$

The probability of detection is obtained by integrating the *pdf* derived from Eq. (3.31) from the threshold value to infinity. Performing the integration in Eq. (3.31) leads to the incomplete Gamma function.

3.6.2. Threshold detection

In practice, the detection threshold, V_T , is found from the probability of false alarm P_{fa}. DiFranco and Rubin1 give a general form relating the threshold and P_{fa} for any number of pulses and non-coherent integration,

$$P_{fa} = 1 - \Gamma_I\left(\frac{V_T}{\sqrt{n_p}}, n_p - 1\right) \tag{3.32}$$

Where, Γ_I is used to denote the incomplete gamma function and it can be expressed as

$$\Gamma_I\left(\frac{V_T}{\sqrt{n_p}}, n_p - 1\right) = \int_0^{V_T\sqrt{n_p}} \frac{e^{-\gamma}\gamma^{n_p-1-1}}{(n_p-1-1)!}\, d\gamma \tag{3.33}$$

The incomplete Gamma function can be approximated by [21]

$$\Gamma_I\left(\frac{V_T}{\sqrt{n_p}}, n_p - 1\right) = 1 - \frac{V_T^{n_p-1}e^{-V_T}}{(n_p-1)!}\left[1 + \frac{n_p-1}{V_T} + \frac{(n_p-1)(n_p-2)}{V_T^2} + \cdots + \frac{(n_p-1)!}{V_T^{n_p-1}}\right] \tag{3.34}$$

The threshold value V_T can then be approximated by the recursive formula used in the Newton-Raphson method. More precisely,

$$V_{T,m} = V_{T,m-1} - \frac{G(V_{T,m-1})}{G'(V_{T,m-1})}\ ; m = 1,2,3,\ldots \tag{3.35}$$

The iteration is terminated when $\left|V_{T,m} - V_{T,m-1}\right| < V_{T,m-1}/10000.0$. The functions G and G' are

$$G\left(V_{T,m}\right) = (0.5)^{\frac{n_p}{n_{fa}}} - \Gamma_1(V_T, n_p) \tag{3.36}$$

$$G'^{(V_{T,m})} = -\frac{e^{-V_T}V_T^{n_p-1}}{(n_p-1)!} \tag{3.37}$$

The initial value for the recursion is

$$V_{T,0} = n_p - \sqrt{n_p} + 2.3\sqrt{-logP_{fa}}\left(\sqrt{-logP_{fa}} + \sqrt{n_p} - 1\right) \tag{3.38}$$

Figure 3.4 shows plots for the threshold value versus the number of integrated pulses for several values of n_{fa}; remember that $P_{fa} \approx \ln(2)(n_p/n_{fa})$.

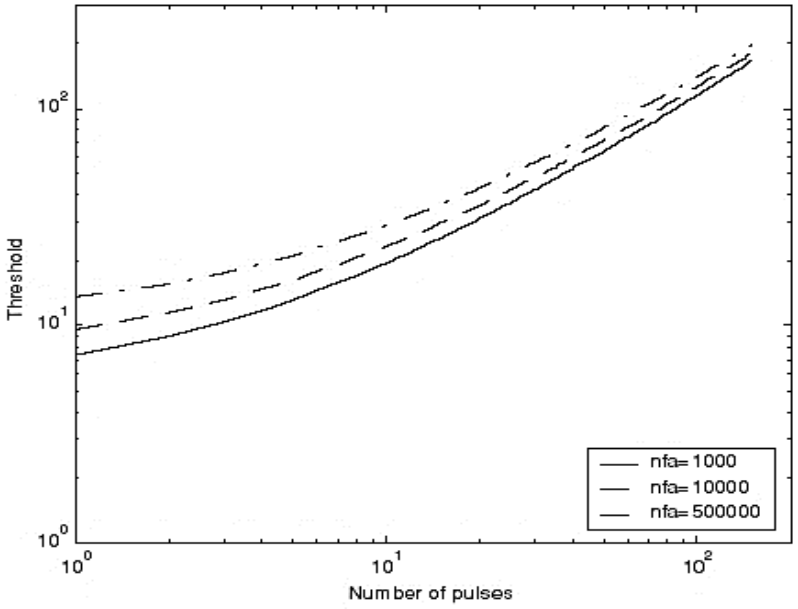

Figure 3.4. Threshold V_T versus n_p for several values of n_{fa}.

3.7. Analysis of Probability of Detection

Denoting the range at which the single pulse SNR is unity (0dB) as R_0 refer to it as the reference range.

Now, for a specific radar, the single pulse SNR at R_0 is defined by the radar equation and it can be written as,

$$(SNR)_{R_0} = \frac{P_t G^2 \lambda^2 \sigma}{(4\pi)^3 R_0^4 k T_0 B F L} \tag{3.39}$$

The single pulse SNR at any range R is

$$(SNR) \quad = \frac{P_t G^2 \lambda^2 \sigma}{(4\pi)^3 R^4 \, k T_0 B F L} \tag{3.40}$$

Dividing Eq. (3.40) by Eq. (3.39) yields

$$\frac{SNR}{(SNR)_{R_0}} = \left(\frac{R_0}{R}\right)^4 \tag{3.41}$$

Therefore, if the range R_0 is known then the SNR at any other range R is

$$(SNR)_{dB} = 40log\left(\frac{R_0}{R}\right) \tag{3.42}$$

3.7.1. Target modelling

In most practical cases there is a relative motion between the radar and an observed target. RCS measured by the radar fluctuates over a period as a function of frequency and the target aspect angle. This observed RCS is referred to as the radar dynamic cross section. At a forward movement the RCS diagram of the airplane is turned in the

reference to the radar set. Caused by the temporal changes of the aim, the amplitude and phase changes effect a strong fluctuation of the reception field strength at the radar antenna.

The target models were introduced by the American mathematician Peter Swerling. Swerling target models give the radar cross-section (RCS) of a given object using a distribution in the location-scale family of the chi-squared distribution. RCS of a reflecting object is based on the chi-square probability density function with specific degrees of freedom. There are four different Swerling models, numbered with the Roman numerals I through IV.

3.7.2. Chi-squared target models

Swerling target models give the radar cross-section (RCS) of a given object using a distribution in the location-scale family of the chi-squared distribution.

$$p(\sigma) = \frac{m}{\Gamma(m)\sigma_{avg}}\left(\frac{m\sigma}{\sigma_{avg}}\right)^{m-1} e^{-\frac{m\sigma}{\sigma_{avg}}} \mathrm{I}_{[0,\infty\}}(\sigma) \tag{3.43}$$

σ_{avg} refers to the mean value of σ. This is not always easy to determine, as certain objects may be viewed the most frequently from a limited range of angles. For instance, a sea-based radar system is most likely to view a ship from the side, the front, and the back, but never the top or the bottom. Here, m is the degree of freedom divided by two.

The degree of freedom used in the chi-squared probability density function is a positive number related to the target model. Values of m between 0.3 and 2 have been found to closely approximate certain simple shapes, such as cylinders or cylinders with fins. Since the ratio of the standard deviation to the mean value of the chi-squared distribution is equal to $m^{-\frac{1}{2}}$, larger values of m will result in smaller fluctuations. If m equals infinity, the target's RCS is non-fluctuating.

The degree of freedom used in the chi-squared probability density function is a positive number related to the target model. The number of independent ways by which a dynamic system can move, without violating any constraint imposed on it, is called number of degrees of freedom. In other words, the number of degrees of freedom can be defined as the minimum number of independent coordinates that can specify the position of the system completely.

3.7.3. Detection of Swerling I target

The echo pulses received from a target on any scan are of constant amplitude throughout the entire scan but are independent (uncorrelated) from scan to scan. This applies to a target that is made up of many independent scatterers of roughly equal areas. As few as half a dozen scattering surfaces can produce this distribution. An echo fluctuation of this type will be referred to as scan-to-scan fluctuation.

3.7.4. Detection of Swerling II target

The Swerling II target is similar to Swerling I, using the same equation, except the RCS values changes faster and varies from pulse to pulse additionally. The Swerling cases I and II applies to a target that is made up of many independent scatterers of roughly equal areas like airplanes. However, in Swerling case II there is no rotating surveillance antenna but a focused onto a target tracking radar.

The probability-density function for the target cross section can also be given by following equation [21]

$$P(\sigma) = \frac{1}{\sigma_{avg}} \exp\left(-\frac{\sigma}{\sigma_{avg}}\right) \quad \sigma \geq 0 \tag{3.44}$$

Where σ_{avg} is the average cross section over all target fluctuations.

But the fluctuations are more rapid than Swerling Model I and are taken to be independent from pulse to pulse instead of from scan to scan.

3.7.5. Detection of Swerling III target

In Swerling Model III, the fluctuation is assumed to be independent from scan to scan just like Swerling Model I. It is a model where the RCS varies according to a Chi-squared probability density function with four degrees of freedom ($m = 2$). This PDF approximates an object with one large scattering surface with several other small scattering surfaces. The probability- density function for the cross section σ is given by the density function

$$P(\sigma) = \frac{4\sigma}{\sigma_{avg}^2} \exp\left(-\frac{2\sigma}{\sigma_{avg}}\right) \tag{3.45}$$

Where σ_{avg} is the average cross section over all target fluctuations. This PDF approximates an object with one large scattering surface with several other small scattering surfaces.

3.7.6. Detection of Swerling IV target

In Swerling Model IV, the fluctuation is assumed to be independent from pulse to pulse just like Swerling Model II. The probability- density function for the cross section σ is given by the density function

$$P(\sigma) = \frac{4\sigma}{\sigma_{avg}^2} \exp\left(-\frac{2\sigma}{\sigma_{avg}}\right) \tag{3.46}$$

Where σ_{avg} is the average cross section over all target fluctuations. It is similar to Swerling III, but the RCS varies from pulse to pulse rather than from scan to scan. Examples include some helicopters and propeller driven aircraft.

3.8. Cumulative Probability of Detection

The cumulative probability of detection refers to detect the target at least once by the time. More precisely, considering a target closing on a scanning radar, where the target is illuminated only during a scan (frame). As the target gets closer to the radar, its probability of detection increases since the SNR is also increased. Suppose that the probability of detection during the nth frame is P_D; then, the cumulative probability of detecting the target at least once during the nth frame (Figure 3.5) is given by

$$P_{C_n} = 1 - \prod_{i=1}^{n} (1 - P_{D_i}) \tag{3.47}$$

P_{D_1} is usually selected to be very small. Clearly, the probability of not detecting the target during the nth frame is $1 - P_{C_n}$. The probability of detection for the ith frame, P_{D_i}, is computed as discussed in the previous section.

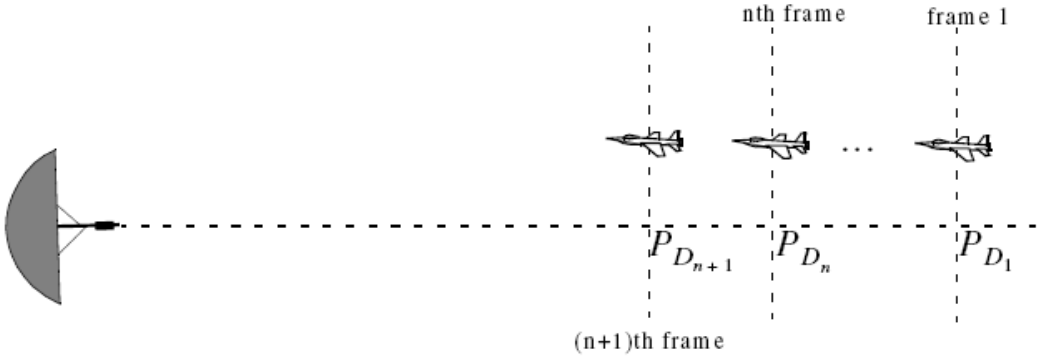

Figure 3.5. Detecting a target in many frames.

3.9. Fundamentals of RADAR Equation

The basic radar equation can be developed as

$$R = \left(\frac{P_t \tau f_r T_i G_t G_r \lambda^2 \sigma}{(4\pi)^3 k T_e F L (SNR)_o} \right)^{\frac{1}{4}} \tag{3.48}$$

Where P_t is peak transmitted power, τ is pulse width, f_r is PRF, T_i is dwell interval, G_t is transmitting antenna gain, G_r is receiving antenna gain, λ is wavelength, σ is target cross section, k is Boltzman's constant, T_e is effective noise temperature, F is system noise figure, L is total system losses and $(SNR)_0$ is the minimum SNR required for detection.

Assuming that the radar parameters such as power, antenna gain, wave length, losses, bandwidth, effective temperature and noise figure are known, the steps should be followed to solve for range shown. It is to be noted that both sides of the bottom half of the figure are identical. Nevertheless, it is seen that there are two paths so that a distinction between scintillating and non-fluctuating target is made.

3.10. Constant False Alarm Rate (CFAR)

The detection threshold is computed so that the radar receiver maintains a constant pre-determined probability of false alarm. The relationship between the threshold value V_T and the probability of false alarm P_{fa} can be written as Eq. (3.49):

$$V_T = \sqrt{2\Psi^2 \ln\left(\frac{1}{P_{fa}}\right)} \tag{3.49}$$

If the noise power ψ^2 is assumed to be constant, then a fixed threshold can satisfy Eq. (3.49). However, due to many reasons this condition is rarely true. Thus, in order to maintain a constant probability of false alarm the threshold value must be continuously updated based on the estimates of the noise variance. The process of continuously changing the threshold value to maintain a constant probability of false alarm is known as Constant False Alarm Rate (CFAR).

Three different types of CFAR processors are primarily used. They are adaptive threshold CFAR, nonparametric CFAR, and nonlinear receiver techniques. Adaptive CFAR assumes that the interference distribution is known and approximates the unknown parameters associated with these distributions. Nonparametric CFAR

processors tend to accommodate unknown interference distributions. Nonlinear receiver techniques attempt to normalize the root mean square amplitude of the interference.

3.11. Cell-Averaging CFAR (single pulse)

The CA-CFAR processor is shown in Figure 3.6. Cell averaging is performed on a series of range and Doppler cells. The echo return for each pulse is detected by a square law detector. In analog implementation these cells are obtained from a tapped delay line. The Cell Under Test (CUT) is the central cell. The immediate neighbors of the CUT are excluded from the averaging process due to possible spillover from the CUT. The threshold value is obtained by multiplying the average estimate from all reference cells by a constant K_0 (used for scaling). A detection is declared in the CUT if

$$Y_1 \geq K_0 Z \tag{3.50}$$

Cell-averaging CFAR assumes that the target of interest is in the CUT and all reference cells contain zero mean independent Gaussian noise of variance ψ^2. Therefore, the output of the reference cells, Z, represents a random variable with gamma probability density function (special case of the Chi-square) with $2M$ degree of freedom. In this case, the gamma pdf is

$$f(z) = \frac{z^{\frac{M}{2}-1} e^{-\frac{z}{2\psi^2}}}{2^{\frac{M}{2}} \psi^M \Gamma\left(\frac{M}{2}\right)} \tag{3.51}$$

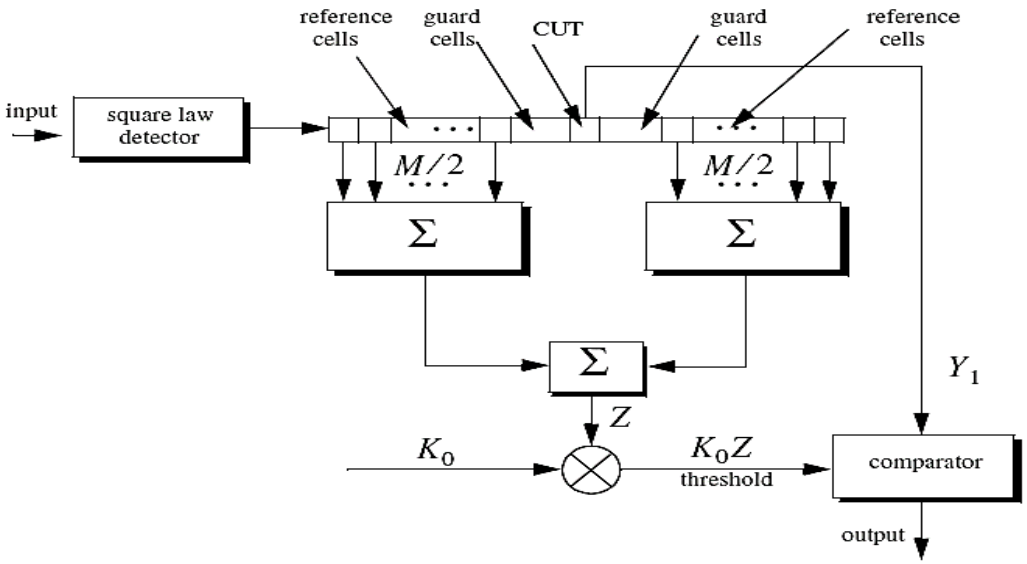

Figure 3.6. Conventional CA-CFAR.

The probability of false alarm corresponding to a fixed threshold was derived earlier. When CA-CFAR is implemented, then the probability of false alarm can be derived from the conditional false alarm probability, which is averaged over all possible values of the threshold in order to achieve an unconditional false alarm probability. The conditional probability of false alarm when $y = V_T$ can be written as [21]

$$P_{fa}(V_T = y) = e^{-\frac{y}{2\psi^2}} \tag{3.52}$$

It follows that the unconditional probability of false alarm is

$$P_{fa} = \int_0^\infty P_{fa}(V_T = y) f(y) dy \tag{3.53}$$

Where $f(y)$ is the pdf of the threshold, which except for the constant K_0 is the same as that defined in Eq. (3.51). Therefore,

$$f(y) = \frac{y^{M-1} e^{\left(-\frac{y}{2K_0\psi^2}\right)}}{(2K_0\psi^2)^M \Gamma(M)} \tag{3.54}$$

Substituting Eqs. (3.53) and (3.51) into Eq. (3.52) yields

$$P_{fa} = \frac{1}{(1 + K_0)^M} \tag{3.55}$$

It is seen that the probability of false alarm is now independent of the noise power, which is the objective of CFAR processing.

3.12. Cell-Averaging CFAR with Non-Coherent Integration

Generally, CFAR averaging is often implemented after non-coherent integration which can be shown in Figure 3.7. The output of each reference cell is the sum of n_p squared envelopes. It follows that the total number of summed reference samples is Mn_p. The output Y_1 is also the sum of n_p squared envelopes. When noise alone is present in the CUT, Y_1 is random variable whose pdf is a gamma distribution with $2n_p$ degrees of freedom. Additionally the summed output of the reference cells is the sum of Mn_p squared envelopes. Thus, Z is also a random variable who has a gamma pdf with $2Mn_p$ degrees of freedom.

The probability of false alarm is then equal to the probability that the ratio Y_1/Z exceeds the threshold. Now, we can write,

$$P_{fa} = Prob\left\{\frac{Y_1}{Z} > K_1\right\} \tag{3.56}$$

From the above equation it is clear that joint pdf for the ratio Y_1/Z must be found out. But, it can be avoided if P_{fa} is first computed for a fixed threshold value V_T, then averaged over all possible value of the threshold. Therefore, the conditional probability of false alarm when $y = V_T$ be $P_{fa}(V_T = y)$. It follows that the unconditional false alarm probability is given by

$$P_{fa} = \int_0^\infty P_{fa}(V_T = y) f(y) dy \tag{3.57}$$

Where $f(y)$ is the pdf of the threshold. In view of this, the probability density function describing the random variable $K_1 Z$ is given by

$$f(y) = \frac{(y/K_1)^{Mn_p - 1} e^{\left(-\frac{y}{2K_0\psi^2}\right)}}{(2\psi^2)^{Mn_p} \mathrm{K}_1 \Gamma(Mn_p)} \tag{3.58}$$

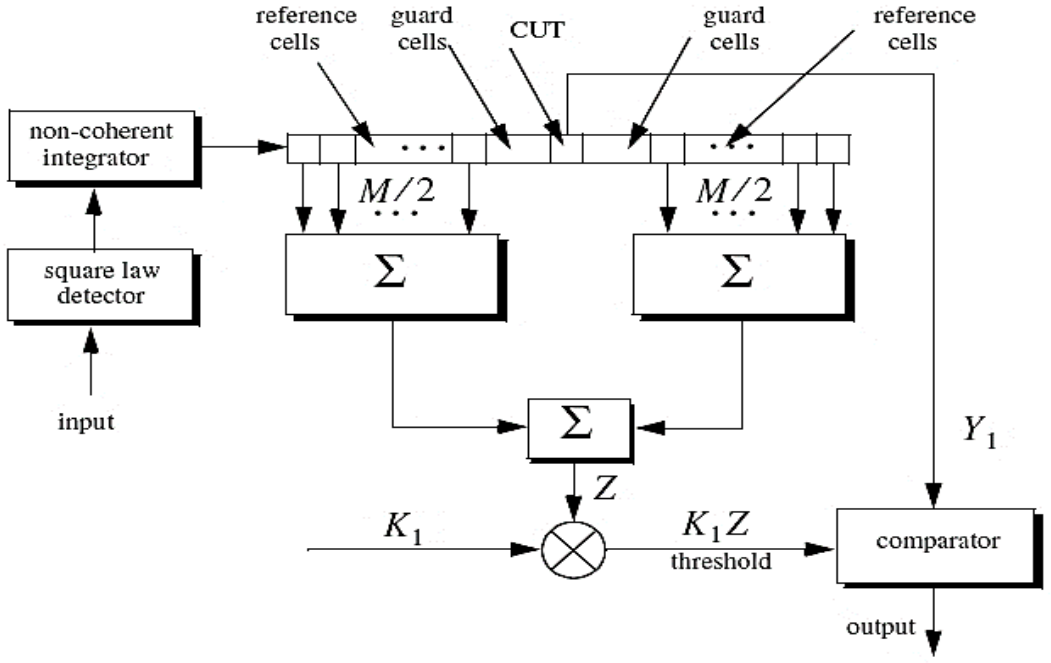

Figure 3.7. CA-CFAR with non-coherent integration.

3.13 Conclusion

This chapter describes the methodology in detail. Various mathematical analysis are explained here regarding this thesis. Analysis of target models and their various behaviors with different parameters are discussed here. Performance analysis based on the simulation are shown in the next chapter.

CHAPTER FOUR

SIMULATION FOR EVALUATION OF SYSTEM PERFORMANCE

4.1. Introduction

By transmitting electromagnetic energy, a radar system can detect targets in various ranges. Radar return is referred to that energy which is reflected off targets within the search volume. An antenna receives the radar return plus noise. This signal is then processed to determine target characteristics such as range and velocity relative to the radar antenna. For any case if the sample magnitude of the radar return crosses the threshold voltage, then its probability is called the Probability of Detection, P_d. Radar cross section (RCS) can lower the probability of detection for a scatterer which have variations within the cross-section range. Swerling Fluctuating Target Models can describe the fluctuation of a scatterer by four specific cases. This paper has proposed a technique to increase the detection probability of radar for fluctuating targets under various false alarm rate.

Swerling developed a mathematical methodology for calculating the detection of fluctuating targets. Four Swerling target models have been established which are special cases of Chi-Squared target models. In Swerling I, RCS varies with two degrees of freedom according to a Chi-squared probability density function. Swerling I & III treats a target whose radar cross-section is fixed throughout a single scan, but varies independently from scan to scan. But in Swerling II & IV radar cross section varies from pulse to pulse and remain constant through scan to scan. The detection of signals becomes complex when radar returns from non-stationary background noise (or noise plus clutter). A radar target can be represented as a function of time on the basis of a large number of real targets whose return changes in magnitude from low to high. In Constant False Alarm Rate (CFAR), the estimation of the noise power levels from the leading and the trailing reference windows are based on the Cell Averaging (CA) technique. The performance of this detector is analyzed in the cases when the operating environment is ideal and when it includes some of spurious targets along with the target of interest. The primary and the secondary interfering targets are assumed to be fluctuating in accordance

with the four Swerling's models cited above. The theoretical result shows that for various False Alarm rate the probability of detection is different.

4.2. Detection Capability in Presence of False Alarm Rate

The probability of detection P_D can be calculated when a sample R of r(t) will exceed the threshold voltage in the case of noise plus signal,

$$P_D = \int_{V_T}^{\infty} \frac{r}{\Psi^2} I_o\left(\frac{rA}{\Psi^2}\right) \exp(-(r^2 + A^2)/2\Psi^2) dr \tag{4.1}$$

In many cases the radar detection threshold is constantly adjusted as a function of the receiver noise level in order to maintain a constant false alarm rate. For this purpose, Constant False Alarm Rate (CFAR) processors are utilized in order to keep the number of false alarms under control in a variable and unknown background of interference. CFAR processing can cause a loss in the SNR level on the order of 1 dB. The detection threshold is computed so that the radar receiver maintains a constant pre-determined probability of false alarm. A relationship between the threshold value V_T and the probability of false alarm P_{fa} can be defined as:

$$V_T = \sqrt{2\Psi^2 \ln\left(\frac{1}{P_{fa}}\right)} \tag{4.2}$$

The probability of false alarm corresponding to a fixed threshold was derived earlier. When CA-CFAR is implemented, then the probability of false alarm can be derived from the conditional false alarm probability, which is averaged over all possible values of the threshold in order to achieve an unconditional false alarm probability. The conditional probability of false alarm when $y = V_T$ can be written as

$$P_{fa}(V_T) = e^{-\left(\frac{y}{2\Psi^2}\right)} \tag{4.3}$$

As a result, unconditional probability of false alarm is

$$P_{fa} = \int_0^{\infty} P_{fa}(y) f(y) dy \tag{4.4}$$

Where, $f(y)$ is the *pdf* of the threshold value.

Practically, CFAR averaging is often implemented after non-coherent integration and the output of each reference cell is the sum of squared envelopes.

4.3. Probability of Detection and CFAR Loss in terms of Threshold Voltage

In Signal to Noise Ratio (SNR) level a loss can be occurred due to CFAR processor.

Gamma function is used to determine the probability of false alarm. It is assumed in adaptive CFAR that the interference distribution is familiar here. This type of CFAR also approximates the unknown parameters connected with various interference distributions. CFAR loss depends on gamma function. Incomplete gamma function plays an important role in maintaining threshold voltage as well as probability of detection. Changing the value of gamma function can improve the probability of detection for various Swerling Models which is proposed here. This research has proposed a technique to compare various losses due to CFAR in terms of different gamma function in presence of different number of pulses integrated for four Swerling Models.

The Chi-square distribution is applied to a wide range of targets, its *pdf* of cross section can be written as,

$$f(\sigma) = \frac{m}{\Gamma(m)\sigma_{avg}} \left(\frac{m\sigma}{\sigma_{avg}}\right)^{m-1} e^{-\frac{m\sigma}{\sigma_{avg}}} \tag{4.5}$$

Where, $\Gamma(m)$ is the gamma function of argument m and σ_{avg} is the average value. As the degree gets larger the distribution corresponds to constrained Radar Cross Section (RCS) values. The limit m tends to ∞ corresponds to a constrained RCS target.

Detection of signals threshold is constantly balanced as a function of the receiver noise level in different cases to maintain a constant false alarm rate [5]. In Signal to Noise Ratio (SNR) level a loss of 1 dB can be occurred due to CFAR processor.

In order to maintain a fixed predetermined probability of false alarm, the threshold of detection is calculated. A relationship between the threshold value V_T and the probability of false alarm P_{fa} can be shown as:

$$V_T = \sqrt{2\Psi^2 \ln\left(\frac{1}{P_{fa}}\right)} \tag{4.6}$$

If the noise power Ψ^2 is assumed to be constant, then a fixed threshold can satisfy the above equation. However, due to many reasons this condition is rarely true. In order to maintain a constant probability of false alarm the threshold value must be continuously updated based on the estimates of the noise variance. The method of continuously changing the threshold value to maintain a fixed probability of false alarm is known as Constant False Alarm Rate (CFAR).

The Swerling models were introduced to model a variety of target reflections that occur over the radar integration interval. In Swerling model I & II where the signal amplitudes are fully correlated over the incoherent integration interval but are independent from one

integration interval to the next. In Swerling model II & IV the signal amplitudes are uncorrelated from pulse to pulse throughout the integration interval.

The probability of false alarm corresponding to a fixed threshold was derived earlier. When CA-CFAR is implemented, then the probability of false alarm can be derived from the conditional false alarm probability, which is averaged over all possible values of the threshold in order to achieve an unconditional false alarm probability. The conditional probability of false alarm when $y = V_T$ can be written as

$$P_{fa}(V_T) = e^{-\left(\frac{y}{2\Psi^2}\right)} \tag{4.7}$$

As a result, unconditional probability of false alarm is

$$P_{fa} = \int_0^\infty P_{fa}(y) f(y) dy \tag{4.8}$$

Where, $f(y)$ is the *pdf* of the threshold value.

In target detection, threshold V_T can be determined from probability of false alarm, P_{fa}. For any number of pulses and non coherent integration DiFranco & Rubin give a standard form relating threshold and probability of false alarm.

$$P_{fa} = 1 - \Gamma_I\left(\frac{V_T}{\sqrt{n_p}}, n_p - 1\right) \tag{4.9}$$

Where, Γ_I is used to denote the incomplete gamma function and it can be expressed as

$$\Gamma_I\left(\frac{V_T}{\sqrt{n_p}}, n_p - 1\right) = \int_0^{V_T\sqrt{n_p}} \frac{e^{-\gamma}\gamma^{n_p-1-1}}{(n_p-1-1)!} d\gamma \tag{4.10}$$

When the number of reference cells in the CA CFAR is greater, the better estimate of the background noise can be found and the loss in detection capability is less. But, there are only finite number of reference cells. As a result, the estimate of the noise is not precise and there will be loss in detectability. The CFAR loss is the signal to noise ratio required when CFAR is employed divided by the signal to noise ratio required for fixed threshold detection. The CFAR loss for pulse detection can be represented as

$$CFAR\ Loss\ (dB) = -\frac{5}{M} log P_{fa} \tag{4.11}$$

4.4. Reduction of Side Lobes using Pulse Compression Technique

Pulse compression is a signal processing technique mainly used in radar, sonar to increase the range resolution as well as the signal to noise ratio. This is achieved by modulating the transmitted pulse and then correlating the received signal with the transmitted pulse.

The main purpose of this technique is to raise the signal to maximum side lobe (signal-to-side lobe) ratio to improve the target detection and range resolution abilities of the radar system. The lower the side lobes, relative to the main lobe peak, the better the main lobe peak can be distinguished. Analog pulse compression involves the use of analog methods to generate and process pulse compression waveforms. Pulse compression is accomplished here by adding frequency modulation to a long pulse at transmission, and by using a matched filter receiver in order to compress the received signal. This technique is called "correlation processing". The second technique is called "stretch processing" and is normally used for extremely wide band radar operations. Digital pulse compression technique consists of frequency coding, binary phase coding (barker code), poly-phase codes, pseudo-random (PRN) codes.

In analog pulse compression technique, the output of the matched filter, $y(t)$ is the compressed pulse which is just the inverse Fourier transform of the product of the signal spectrum and the matched filter response.

$$y(t) = \frac{1}{2\pi} \int_{-\infty}^{\infty} |H(\omega)|^2 \exp(j\omega t)\, dw \tag{4.12}$$

Here received echo is fed into a matched filter whose frequency response is the complex conjugate $H^*(\omega)$ of the coding filter. A filter is also matched if the signal is the complex conjugate of the time inverse of the filter's impulse response [4, 5]. This is achieved by applying the time inverse of the received signal to the pulse-compression filter. The output of this matched filter is given by the convolution of the signal $h(t)$ with the conjugate impulse response $h^*(-t)$ of the matched filter

$$y(t) = \int_{-\infty}^{\infty} h(\tau)\, h^*(t-\tau) d\tau \tag{4.13}$$

Pulse compression technique is the practical implementation of a matched filter system as shown schematically in the figure below.

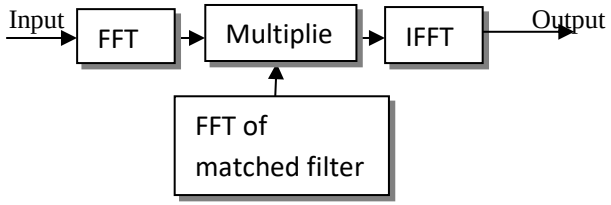

Figure 4.1. A block diagram of Analog Pulse Compression based on FFT and IFFT.

In digital pulse compression technique (Barker code), a relatively long pulse of width τ' is divided into *N* smaller pulses, each is of width $\Delta\tau = \tau'/N$. Then, the phase of each sub-pulse is randomly chosen as either 0 or π radians relative to some CW reference signal. It is customary to characterize a sub-pulse that has 0 phase (amplitude of +1 Volt) as either "1" or "+."

The compression ratio associated with binary phase codes is equal to $\xi = \tau'/\Delta\tau$, and the peak value is *N* times larger than that of the long pulse.

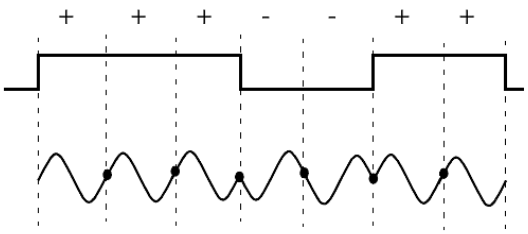

Figure 4.2. Binary Phase Code of length 7.

The most side lobe reduction offered by a Barker code is $-22.3\ dB$, which may not be sufficient for the desired radar application. However, Barker codes can be combined to generate much longer codes. In this case, a B_m code can be used within a B_n code (*m* within *n*) to generate a code of length *mn* . The compression ratio for the combined B_{mn} code is equal to *mn.* Some side lobes of a Barker code autocorrelation function can be reduced to zero if the matched filter is followed by a linear transversal filter with impulse response given by

$$h(t) = \sum_{K=-N}^{N} \beta_k \delta(t - 2k\Delta\tau) \tag{4.14}$$

Where *N* is the filter's order, the coefficients $\beta_k (\beta_k = \beta_{-k})$ are to be determined, $\delta(\bullet)$ is the delta function, and $\Delta\tau$ is the Barker code sub-pulse width. A filter of N order produces N zero side lobes on either side of the main lobe. The main lobe amplitude and width do not change. Let us consider the input of the matched filter is B_{11} and assume order N=4. The auto correlation for a B_{11} code is

$$B_{11} = \{-1,0,-1,0,-1,0,-1,0,-1,0,-1,0,-1,0,-1,0,-1-1,0\}$$

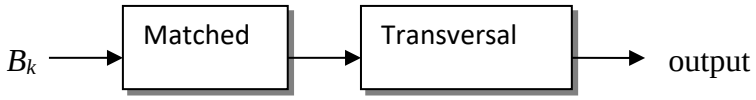

Figure 4.3. Block diagram of barker code followed by a Transversal filter.

4.5. Atmospheric Attenuation of Propagated Radio Wave

During the propagation of RADAR signals in the form of electromagnetic waves in different layers of earth atmosphere, it can be affected by various parameters of the atmosphere. There are different layers in atmosphere depending on temperature. They are troposphere, stratosphere, mesosphere and thermosphere and exosphere. Due to refractive effect the propagated waves bend downward for travelling in different region. Various parameters in atmosphere such as temperature, pressure, water vapor and gaseous content can change the dielectric constant of the medium which is directly related to refractive effect. Because of change in atmospheric behavior radar signals normally lose their energy. This type of loss is usually called as atmospheric attenuation. Natural phenomenon like fog, rain, cloud or dust can significantly increase the atmospheric attenuation. Again, when propagated radar signal reflected from the surface of earth, it losses energy in terms of amplitude and there occurs a change in phase of the travelled wave. Performance analysis of detection capability of radar for the losses due to refraction and reflection has been demonstrated here by doing different types of simulations.

For wide range of targets, the Chi-square distribution *pdf* can be written as

$$f(\sigma) = \frac{m}{\Gamma(m)\sigma_{avg}}\left(\frac{m\sigma}{\sigma_{avg}}\right)^{m-1} e^{-\frac{m\sigma}{\sigma_{avg}}} \tag{4.15}$$

Where, $\Gamma(m)$ denotes gamma function with argument m and σ_{avg} is the average value. The distribution corresponds to constrained Radar Cross Section (RCS) values when the degree of freedom gets larger. The limit m tends to infinity corresponds to a constrained RCS target. Swerling models were introduced to define a target model including variety of target reflections occurring over the radar integration interval. In Swerling Model I & II where the signal amplitudes are fully correlated over the incoherent integration interval but are independent from one integration interval to the next. In Swerling Model II & IV the signal amplitudes are uncorrelated from pulse to pulse throughout the integration interval.

The propagated radar signal deviates from straight line of travelling due to the variation of the index of refraction. The index of refraction can be written as

$$n = \frac{c}{v} \tag{4.16}$$

where c denotes the velocity of electromagnetic waves in free space and v is the propagated wave velocity in the medium.

The index of refraction is generally varied with altitude and near to surface of earth it is almost unity. It normally decreases with increasing value of altitude. From this we can define refractivity gradient in which the index of refraction n changes with altitude$h$. Mathematically the refractivity gradient can be expressed as dn/dh. For this reason, the wave propagating horizontally through the troposphere bend downward. Bending due to refractivity index is only significant when the wave travels long distance through troposphere.

Depending on height refractivity index affects propagated waves in two different ways. Detection capability of RADAR can be varied due to the limitations caused by refraction. In this case, an error occurs while measuring the elevation angle. In general, the index of refractivity remains constant near to the earth surface. Due to the change of temperature and humidity close to the earth's surface a serious variation can be observed in refractivity index.

Radar signal also experiences loss of energy due to reflection to the various surfaces. Probability of detection can be changed due to the reflection coefficient depending on the various surface, its dielectric constant and on the grazing angle of Radar. The reflection coefficients for vertical polarization can be shown as

$$\Gamma_v = \frac{\varepsilon sin\psi_g - \sqrt{\varepsilon - \left(cos\psi_g\right)^2}}{\varepsilon sin\psi_g + \sqrt{\varepsilon - \left(cos\psi_g\right)^2}} \tag{4.17}$$

The horizontal polarization reflection coefficients can be written as

$$\Gamma_h = \frac{sin\psi_g - \sqrt{\varepsilon - \left(cos\psi_g\right)^2}}{sin\psi_g + \sqrt{\varepsilon - \left(cos\psi_g\right)^2}} \tag{4.18}$$

Where ψ_g is the grazing angle and ε is the complex dielectric constant of the surface. The overall reflection coefficient is normally affected by the round earth divergence factor. Because of the earth curvature the reflected wave diverges when an

electromagnetic wave is incident on a round earth surface. The reflected energy is not able to be in focus of the track due to divergence. As a result the radar power density is decreased. The equation of divergence factor can be found by using geometrical considerations. The approximation for the divergence factor can be given by

$$D \approx \frac{1}{\sqrt{1+\frac{2r_1r_2}{r_e r sin\psi_g}}} \tag{4.19}$$

As previously discussed the refractivity changes with altitude. From the model of Bean and Thayer it is observed that refractivity has a fairly linear height gradient to about 1 km above ground, then decays exponentially beyond that. The refractivity depends on surface condition below an altitude of 9 km. The refractivity is relatively surface condition independent above 9 km. The proposed model of refractivity on altitude from Bean and Thayer [9] can be written as

$$N(h) = \begin{cases} N_s + (h-h_s)\Delta N \\ N_1 e^{-\frac{(h-h_s-1000)}{H}} \\ 105e^{-\frac{(h-9000)}{7023}} \end{cases} \tag{4.20}$$

Where, N_s = refractivity at the surface

N_1 = refractivity at 1000 m above the surface

ΔN = refractivity linear decay constant

H = refractivity exponential decay constant

The modified model [6] of refractivity based on the breakpoint of altitude can be written as

$$N(h) = N_s e^{-\frac{(h-h_s)}{H_b}} \tag{4.21}$$

Where $$H_b = \frac{h_b-h_s}{\ln\left(\frac{N_s}{N_b}\right)} \tag{4.22}$$

In this modified model a breakpoint is selected above 9 km height to which the propagated waves pass through.

4.6. Conclusion

Limits of the methodology are scientifically assessed and simulations are done to evaluate the system performance of Radar system in this chapter. Final results taken from simulations are discussed in the next chapter.

CHAPTER FIVE

RESULTS AND DISCUSSIONS

5.1. Introduction

Simulation is carried out for different Swerling Models in terms of fluctuating target to improve the detection capability of RADAR in various condition by applying different techniques. The research includes four different segments to increase probability of detection for radar system. Different results are found for various types of Swerling Models for the proposed system consisting of detection capability in presence of False Alarm Rate, finding the probability of detection and CFAR loss in terms of threshold voltage, reduction of side lobes using pulse compression technique and determining the atmospheric attenuation of propagated wave.

5.2. Detection Capability in Presence of False Alarm Rate

Comparative analysis has been done for P_d vs CFAR for four types of Swerling model. Conventional Cell Averaging CFAR has been used here for the simulation. For different false alarm rate the probability of detection will be different if the Signal to Noise Ratio (SNR dB) varies firmly. Probability of detection and constant false alarm rate have been calculated using conventional formula. For every model of Swerling, P_d and CFAR have simulated and compared. Detection probability of target detection was found out with respect to Signal to Noise Ratio (SNR). Constant false alarm rate was calculated and compared for different Swerling model on fluctuating target. Figure 5.1 shows the general characteristics curve of probability of detection with respect to various changes in Signal to Noise Ratio.

The analytical approach presented in chapter four follows various parameters. Different values of system parameters are used to simulate to find out desired results. Values of these parameters are set in a systematic way, as a result the final output from simulation are similar to the output in the cases of practical scenario.

Table 5.1. System parameters

Parameter	Symbol	Value
False alarm number	n_{fa}	10^5
Integrated pulses	n_p	1~100
Grazing angle	ψ	0~90 $degree$
Signal to Noise Ratio	snr	-10~70 dB
Surface refractivity	N_s	350 $N-unit$
Cell array	M	0~40
Dielectric constant	ε	65
Target surface altitude	h_s	6000 m
Height at break point	h_b	40 kft
Refractivity at break point	N_b	66.65 $N-unit$

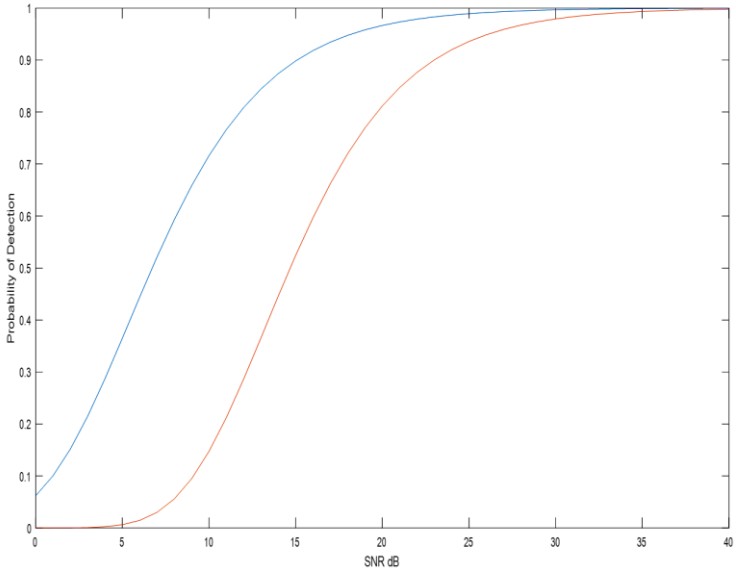

Figure 5.1. Probability of Detection vs SNR(dB) for different number of pulses.

From Figure 5.2 it is seen $t_h$at for different CFAR, the value of probability of detection is different. For simplicity we can assume the value of CFAR is 2 unit and 10 unit to determine probability of detection in each case of Swerling.

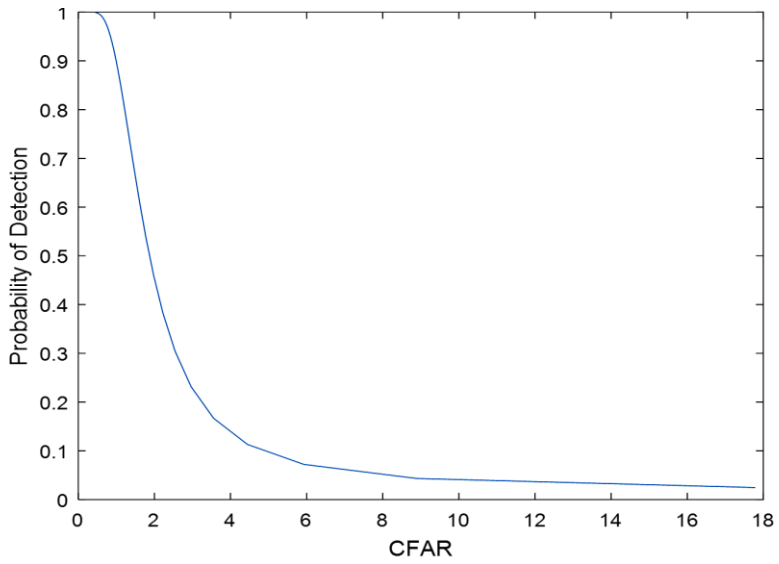

Figure 5.2.a. Probability of Detection vs CFAR for Swerling Model I.

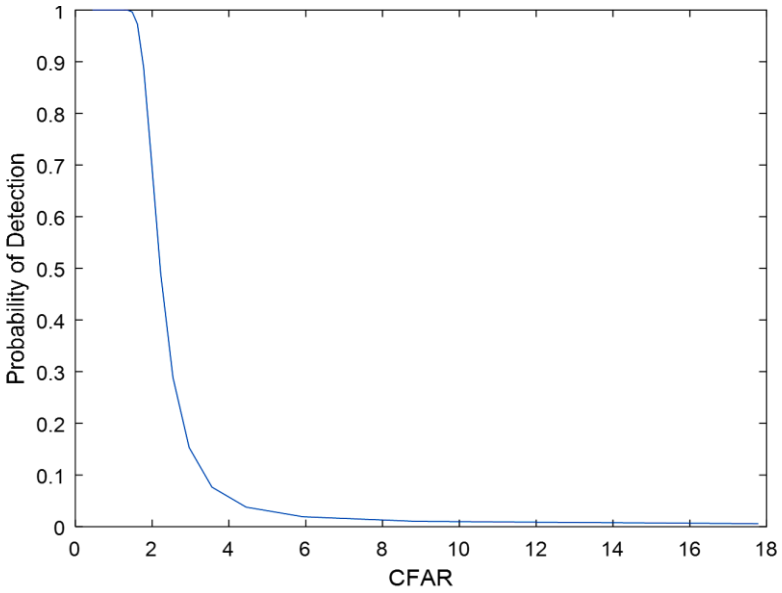

Figure 5.2.b. Probability of Detection vs CFAR for Swerling Model II.

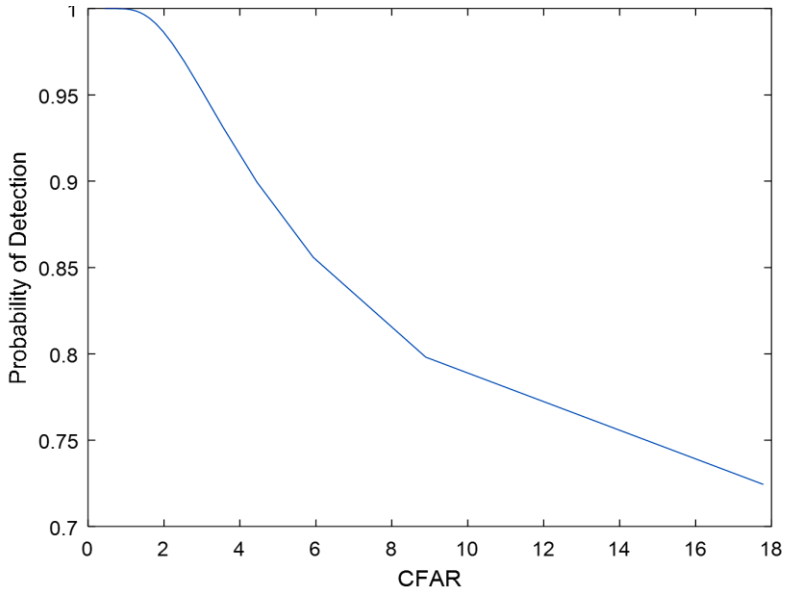

Figure 5.2.c. Probability of Detection vs CFAR for Swerling Model III.

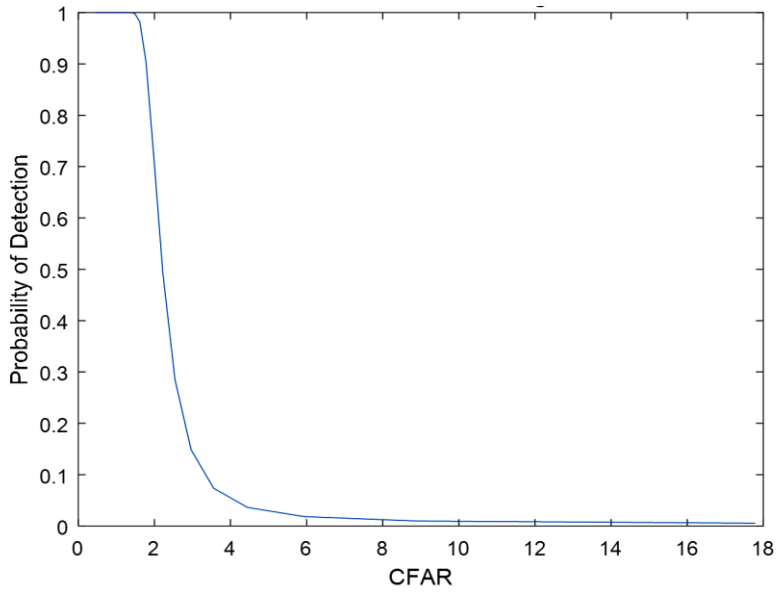

Figure 5.2.d. Probability of Detection vs CFAR for Swerling Model IV.

Table 5.2. Probability of Detection vs CFAR

Swerling Model	***Observation A***		***Observation B***		***Observation C***		***Observation D***	
	CFAR (V)	P_d	CFAR (V)	P_d	CFAR (V)	P_d	CFAR (V)	P_d
I	2	0.46	4	0.1	6	0.06	10	0.04
II	2	0.7	4	0.05	6	0.02	10	0.01
III	2	0.98	4	0.92	6	0.85	10	0.77
IV	2	0.6	4	0.05	6	0.03	10	0.01

Four observations have been taken from the Table 5.2 for random values of CFAR. It is shown that for increasing rate of CFAR the probability of detection is decreasing. As a result, at low CFAR the value of P_D will be maximum. If we consider a certain value of CFAR it is seen that for Swerling model III, the probability of detection is higher than any other model. CFAR should be kept within a moderate range to create a balance with threshold voltage. The optimal value for CFAR is 4 volt. It is observed that Swerling model II has the second highest value of P_D in this comparison which pointed out in the above table.

5.3. Probability of Detection and CFAR Loss in terms of Threshold Voltage

For different Swerling Model Simulation has been carried out in terms of fluctuating target. Conventional Cell Averaging CFAR has been used here. Probability of detection is different for different false alarm rate if the Signal to Noise Ratio (SNR dB) varies firmly. For every model of Swerling, CFAR loss has been simulated and compared. Detection probability of target detection can be found in terms of Signal to Noise Ratio (SNR). From probability of false alarm, loss occurred due to Constant false alarm rate was calculated and compared with respect to gamma function for different Swerling model on fluctuating target.

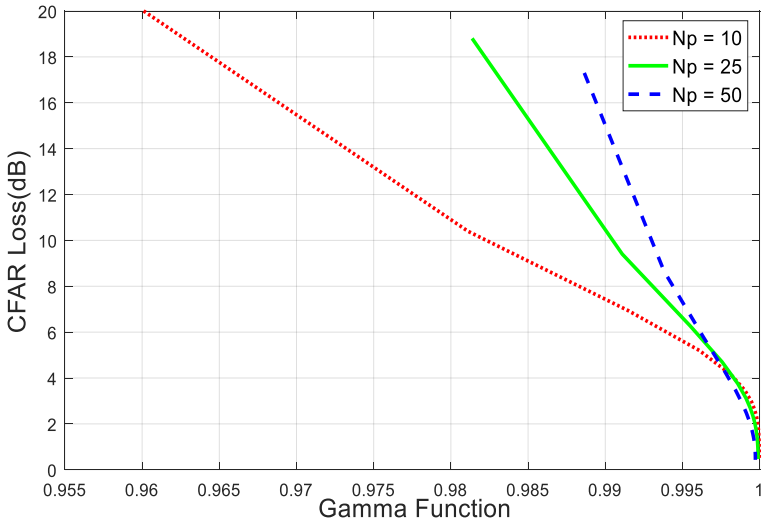

Figure 5.3. CFAR Loss vs Gamma Parameter for Swerling Model I.

In our investigation, comparison has been shown for CFAR loss vs gamma function for four types of Swerling model. From Figure 5.3 it is seen that the value of CFAR loss is decreasing with increasing of gamma function for Swerling model I. In this case CFAR

loss can be reduced if the number of pulse is comparatively less. For different number of pulses characteristics of CFAR loss is different. When the integrated pulse number is minimum, CFAR loss is maximum. Gamma parameter is related to threshold detection and it directly effects the CFAR loss in RADAR system.

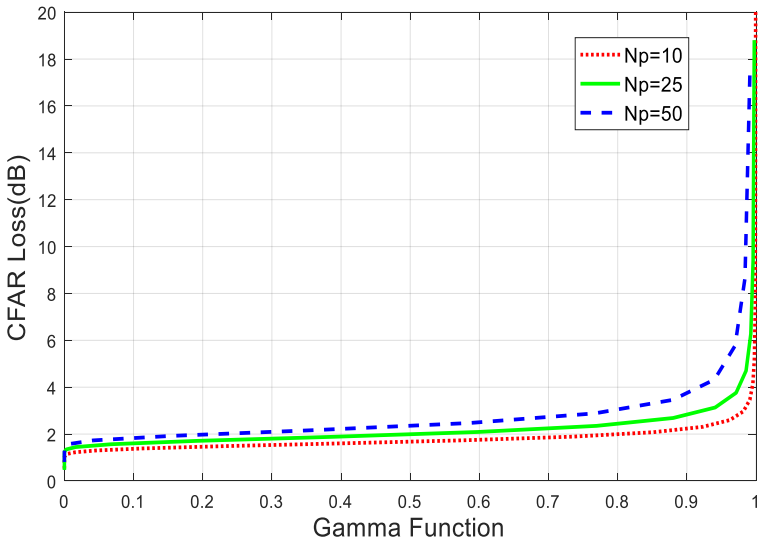

Figure 5.4. CFAR Loss vs Gamma Parameter for Swerling Model II.

From Figure 5.4 it is clearly seen that the value of CFAR loss is sharply increasing after a certain period of gamma function for Swerling model II. The curve of CFAR loss slightly varies from others for different number of pulses.

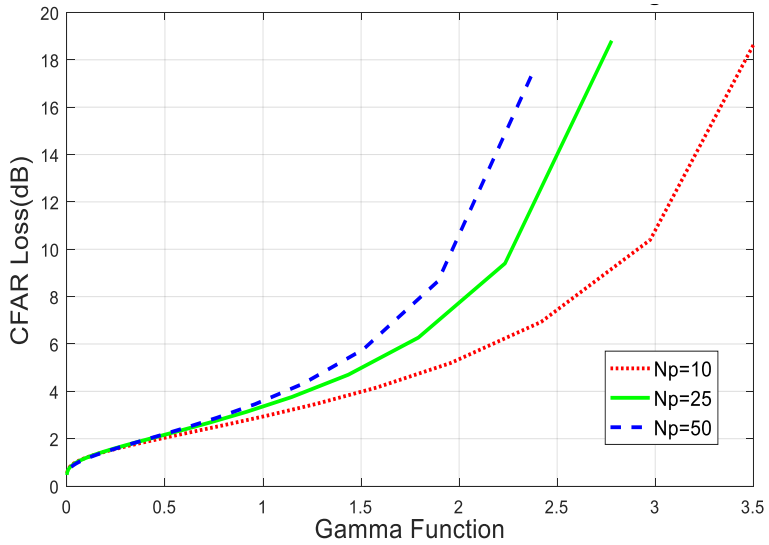

Figure 5.5. CFAR Loss vs Gamma Parameter for Swerling Model III.

It is shown in Figure 5.5 that CFAR loss is increased if the value of gamma function increases for Swerling model III. CFAR loss is comparatively low for less number of pulses.

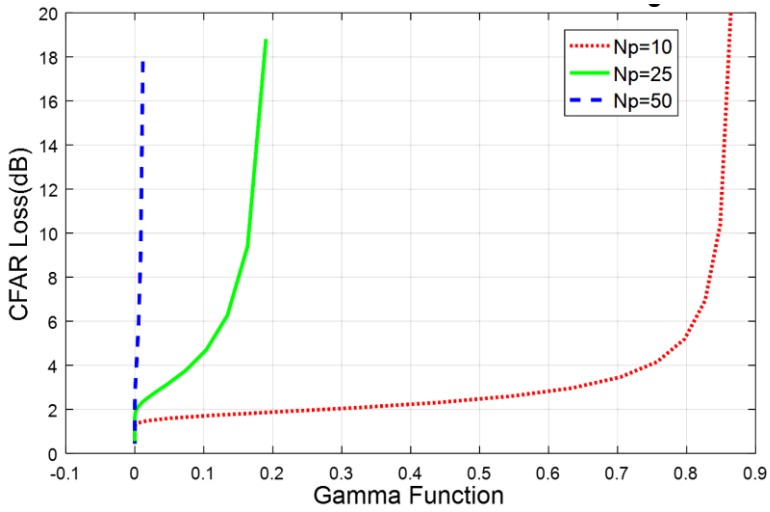

Figure 5.6. CFAR Loss vs Gamma Parameter for Swerling Model IV.

For Swerling model IV from Figure 5.6 it is seen that the curve of CFAR loss shows rapid response in terms of gamma function. For a small value of gamma CFAR loss can be increased sharply up to 20 dB.

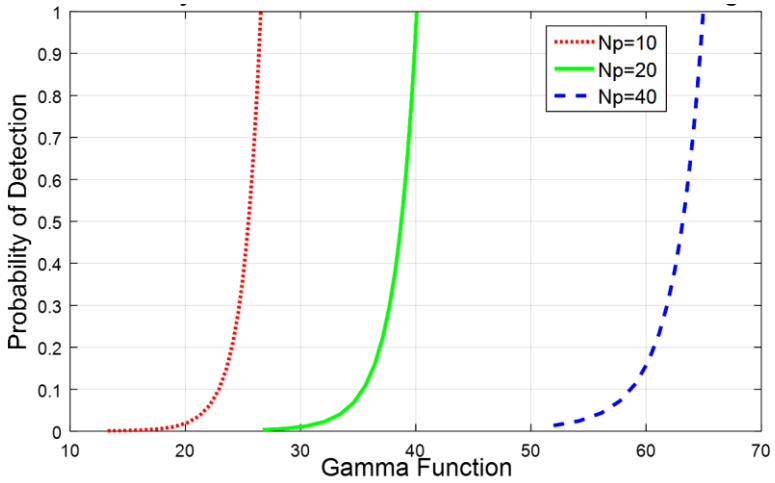

Figure 5.7. Pd vs Gamma Parameter for Swerling Model I.

Probability of detection from Figure 5.7 also depends on gamma parameter. For Swerling model I detection capability of radar increases rapidly for a little change of gamma function shown in Figure 5.7. For different number of pulses the range of gamma parameter is different.

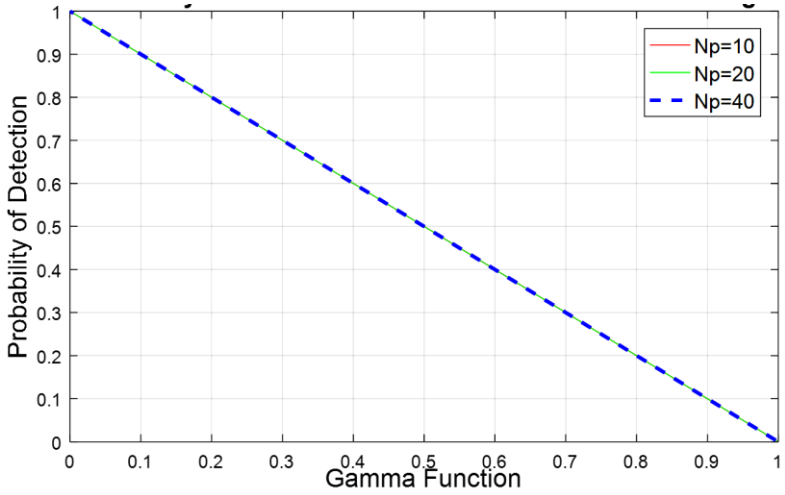

Figure 5.8. Pd vs Gamma Parameter for Swerling Model II.

The fluctuation of targets is independent from pulse to pulse rather than from scan to scan for Swerling model II. From Figure 5.8 it is observed that probability of detection decreases linearly with increasing gamma function. It happens for any number of pulse.

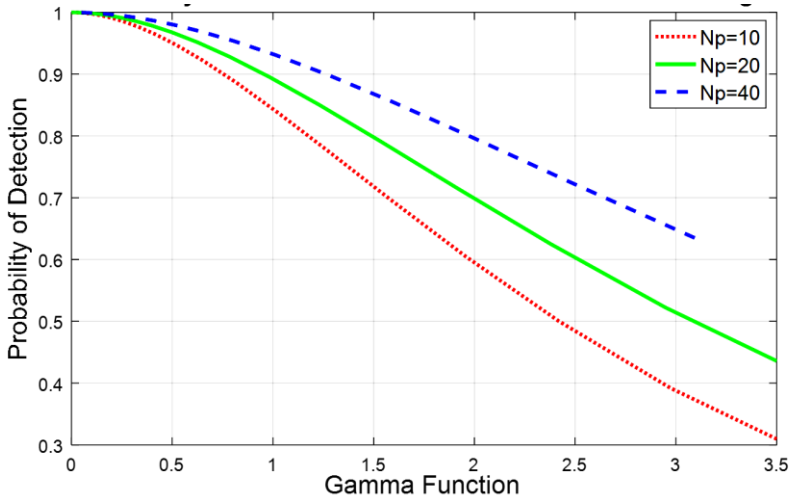

Figure 5.9. Pd vs Gamma Parameter for Swerling Model III.

Probability of detection also decreases with increasing gamma function in Swerling model III. But the behavior of this curve is almost linear in nature. If the number of pulse is higher, the detection capability improves for any values of gamma parameter which is shown in Figure 5.9.

For Swerling model IV, the detection capability rapidly decreases from its highest value with increasing gamma parameter. For different number of pulses the curve shows various behaviors which are mentioned in Figure 5.10.

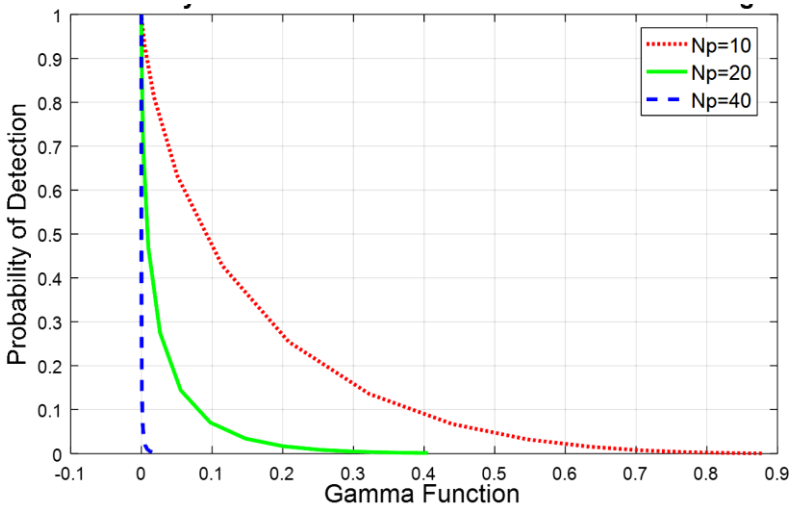

Figure 5.10. Pd vs Gamma Parameter for Swerling Model IV.

It is clear from the figures that there are more CFAR loss for Swerling model II, III & IV if the value of gamma function is increased. For Swerling model I, CFAR loss is less for increasing value of gamma function. Again, gamma function is related to probability of detection in RADAR. At low value of gamma, the CFAR loss is minimum for Swerling model III. It is clear that Swerling model III has the second highest detection capability where the loss due to Constant False Alarm Rate (CFAR) is lower. For Chi square distribution used in probability of detection, gamma is inversely proportional to the pdf. For Swerling model II, III & IV the probability of detection decreases with increasing gamma parameter. For better detection capability, the value of gamma function should be kept as low.

5.4. Reduction of Side Lobes Using Pulse Compression Technique

For analog pulse compression technique simulation was done by using matched filter. For the analog compression we have used chirp frequency of 5.6 GHz and chirp bandwidth of 1GHz. Scattering range of 150 km is also used.

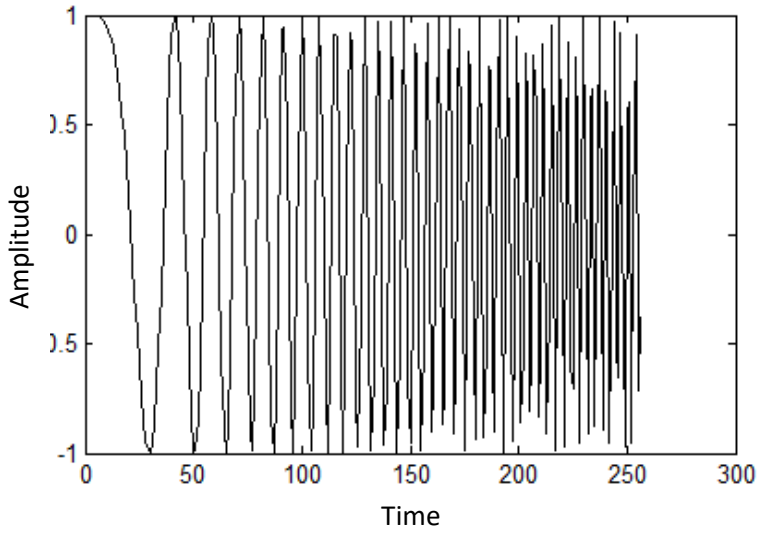

Figure 5.11. Matched Filter Time Domain Response.

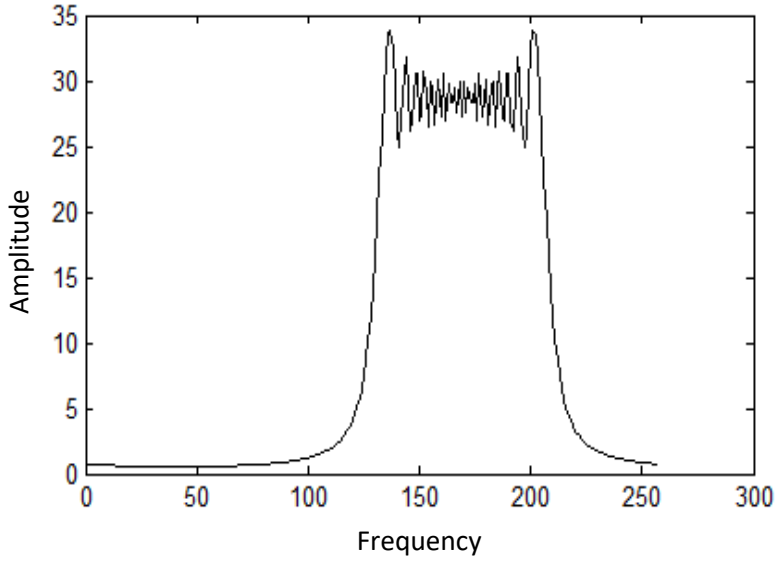

Figure 5.12. Matched Filter Frequency Domain Response.

In digital pulse compression, barker code, auto correlation of binary signal is accomplished. Here barker code of length seven was used. In general, the autocorrelation function (which is an approximation for the matched filter output) for a B_N Barker code will be $2N\Delta\tau$ wide. The main lobe is $2\Delta\tau$ wide; the peak value is equal to N. There are $(N-1)/2$ side lobes on either side of the main lobe. Figure 5.11 and Figure 5.12 show the time domain response and frequency domain response of matched filter respectively. Here by applying Fast Fourier Transform, the frequency domain response of matched filter has been shown.

Figure 5.14 represents the barker code of length seven. By doing the auto correlation of binary signal barker code can be found.

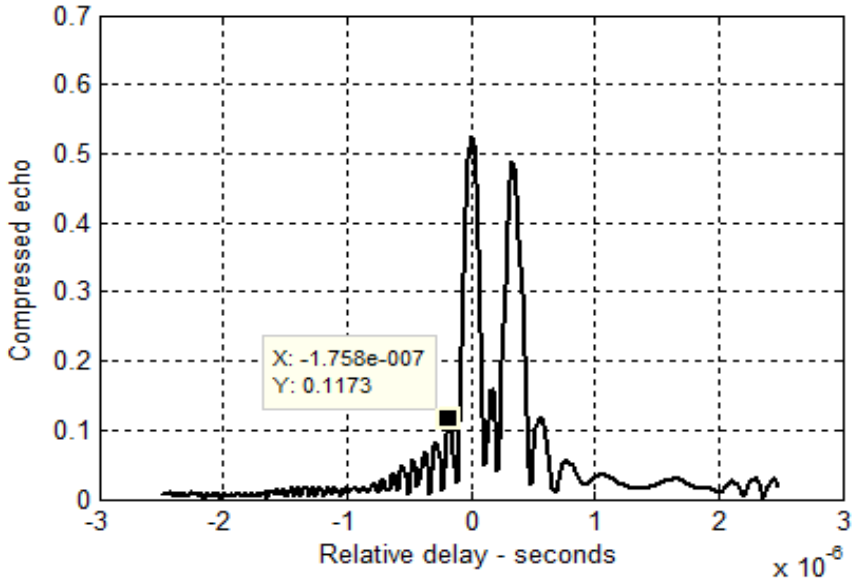

Figure 5.13. Compressed echo using analog pulse compression technique.

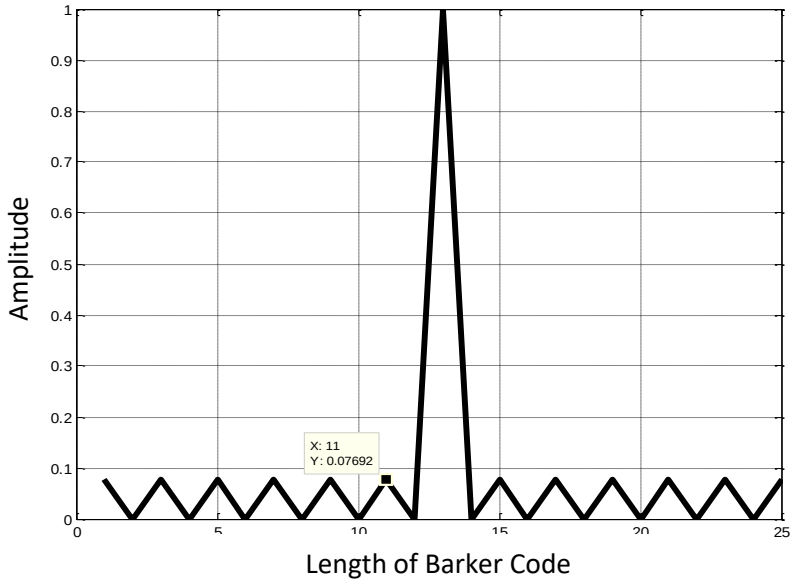

Figure 5.14. Compressed echo using digital pulse compression technique

The output of the matched filter is used as the input of the Transversal filter of order N.

Finally, with this process the desired output of digital pulse compression can be achieved. Side lobes are compared between analog pulse compression technique and digital pulse compression technique by using barker code.

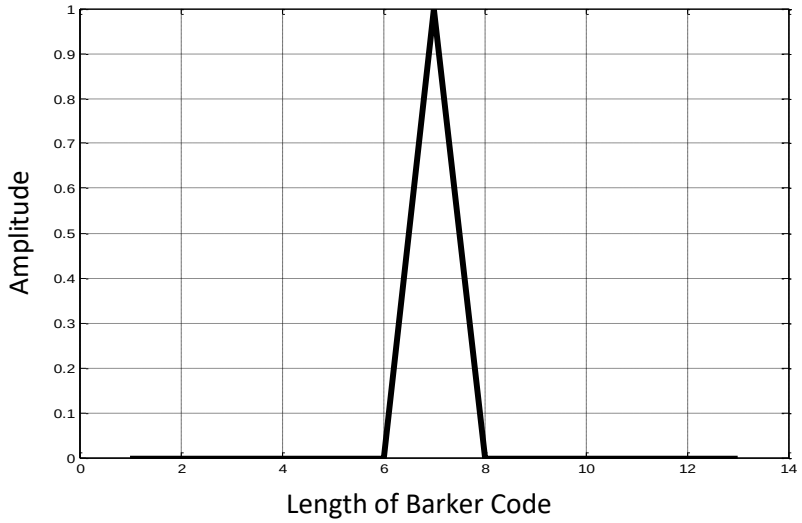

Figure 5.15. Compressed echo using Digital pulse compression followed by transversal filter

Table 5.3. Side Lobes of Different Techniques

Pulse Compression Technique	***Peak Side lobe Level (Volt)***
Analog (using matched filter)	0.1173
Digital (using barker code)	0.07692
Digital (followed by a transversal filter)	Almost zero

From the above figure the side lobes from different pulse compression technique can be seen. The side lobes are different in different pulse compression technique. In digital pulse compression technique, the side lobe is less than the analog pulse compression technique. The side lobe is 0.1173 volt in analog pulse compression using matched filter & it is 0.07692 volt in digital pulse compression using barker code. The peak side lobe is reduced to zero when the transversal filter is used.

5.5. Atmospheric Attenuation of Propagated Wave

For various types of Swerling Models simulation has been carried out in terms of fluctuating target to observe atmospheric attenuation. Most of the attenuation of propagated radar signals occur due to surface reflection and refraction phenomenon of the wave in different layers of earth atmosphere. Horizontal polarization reflection coefficient has been considered for smooth surface reflection. Incident angle of radar is varied for particular complex dielectric constant of the surface. For various ranges of grazing angle simulation has been completed to find out different reflection coefficient.

Detection capability of radar is changed due to the change in reflection coefficient of travelling wave. Loss of energy is observed in this simulation for this type of fluctuation in probability of detection. Another important parameter in atmospheric attenuation is the bending properties of radar wave. Refractivity has been observed in terms of various altitude from the surface. A range of altitude of 0 to 50 kft is used for the simulation. Breakpoint has been considered within this range. For the refraction properties in various altitude radar signal also suffers a loss. It severely effects on detection capability. Simulation has been carried out also for detection capability of radar vs refractivity.

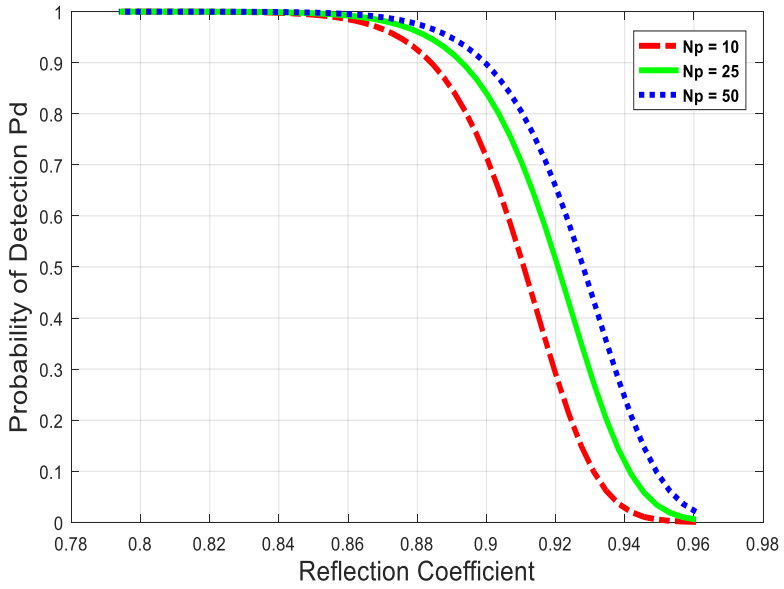

Figure 5.16. Pd vs Reflection Coefficient for Swerling Model I

From the simulation for different types of Swerling model, the behavior of detection capability of RADAR in terms of reflection coefficient and refractivity has been observed carefully. After this, a comparison has been shown for different probability of detection for four different target models. From Figure 5.16 it is seen that the value of probability of detection, P_d is decreasing with increasing value of reflection coefficient for Swerling target model I.

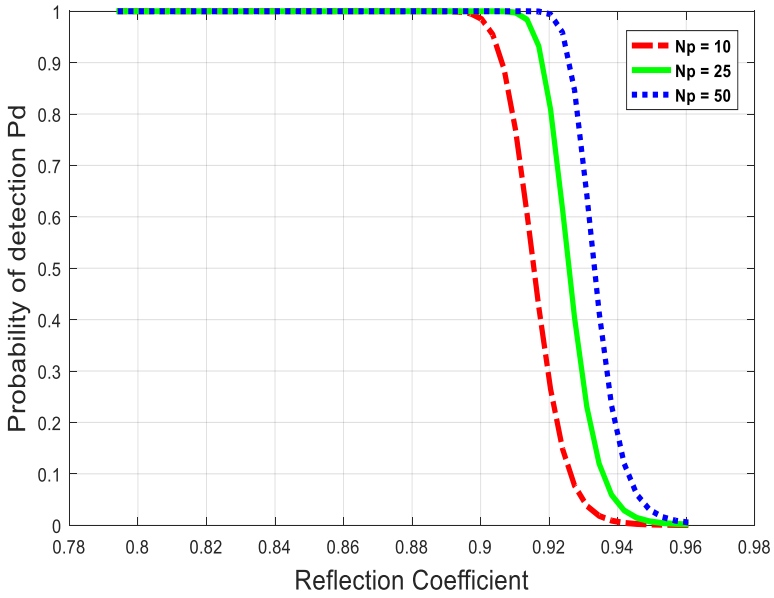

Figure 5.17. Pd vs Reflection Coefficient for Swerling Model II

It is seen from Figure 5.17 that detection capability of RADAR falls sharply for higher values of reflection coefficient when the simulation is carried out for Swerling model II. The curve of probability of detection varies slightly from others for different number of pulses.

Loss in detection capability due to atmospheric attenuation in terms of reflection increases when the value of coefficient is higher as shown in Figure 5.18. It is clear that for various number of pulses the value of P_d is different for Swerling model III.

Probability of detection of propagated wave is higher for the lower value of reflection coefficient and it can be observed from Swerling model IV. The change of detection capability falls sharply for the increasing values of reflection coefficient for different number of integrated pulse which is shown in Figure 5.19. For all target models it is similar.

Due to refractivity in earth atmosphere detection capability follows a non-linear equation which is shown in Figure 5.20. The value of P_d is maximum when there is almost no refraction. But in practical cases loss due to attenuation for refractivity occurs in different layers of earth atmosphere.

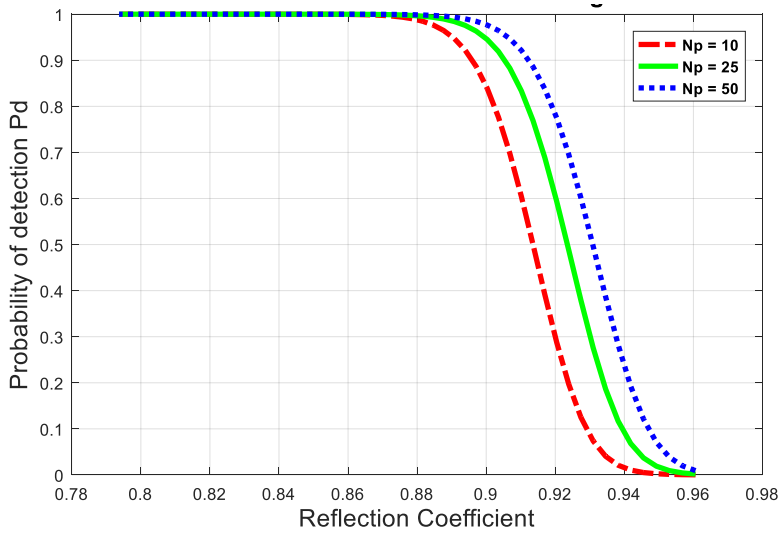

Figure 5.18. Pd vs Reflection Coefficient for Swerling Model III

The detection capability may vary for various number of pulses which is observed for Swerling model I. The variation happens slowly with increasing value of refractivity.

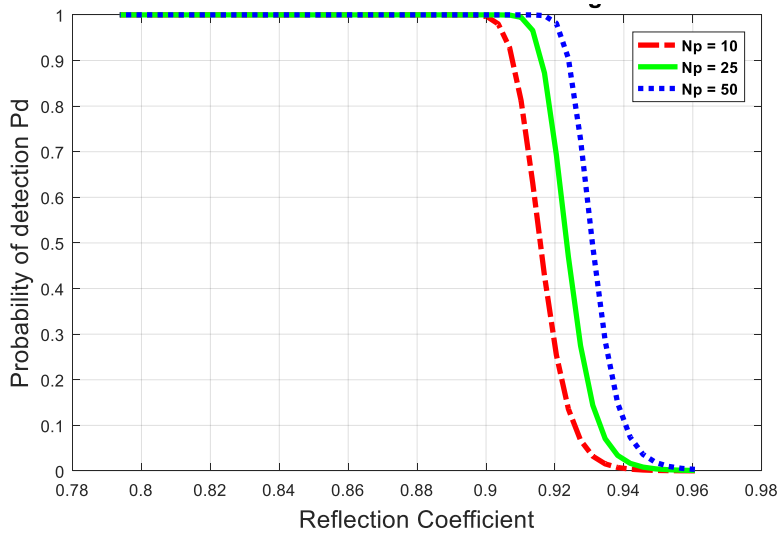

Figure 5.19. Pd vs Reflection Coefficient for Swerling Model IV

In this case simulation has been carried out within a range of altitude from 0 to 40 kft and target surface altitude is assumed to be around 20 kft. For Swerling model II, the probability of detection of RADAR remains as maximum value for the range of refractivity up to 400 N-units shown in Figure 5.21.

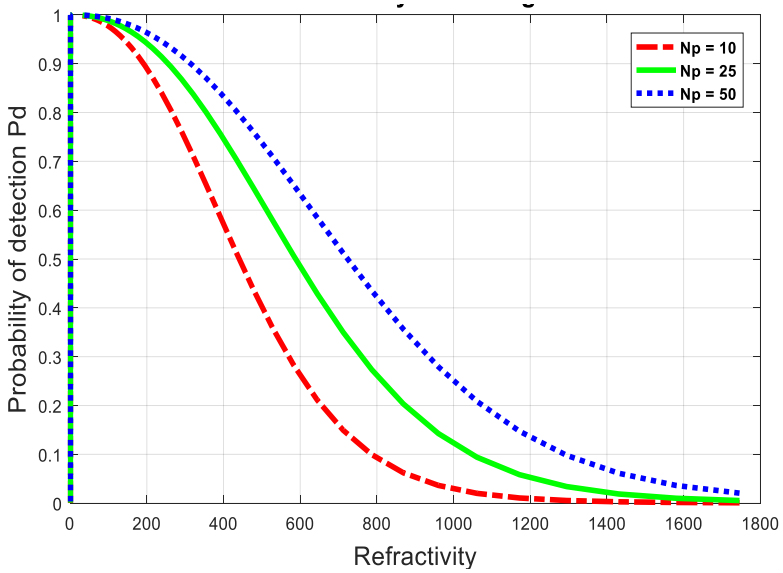

Figure 5.20. Pd vs Refractivity for Swerling Model I

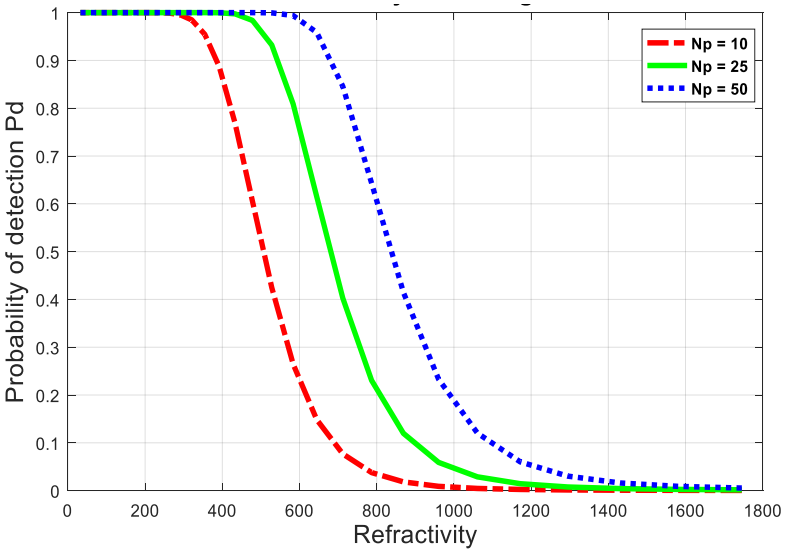

Figure 5.21. Pd vs Refractivity for Swerling Model II

If the number of pulses is increased the detection capability is much better in terms of refraction in the earth atmosphere. For Swerling model III the probability of detection decreases slowly with larger values of refractivity. When the number of pulse is assumed to be as 50, the detection capability is much more higher than the other types of pulses used here as shown in Figure 5.22.

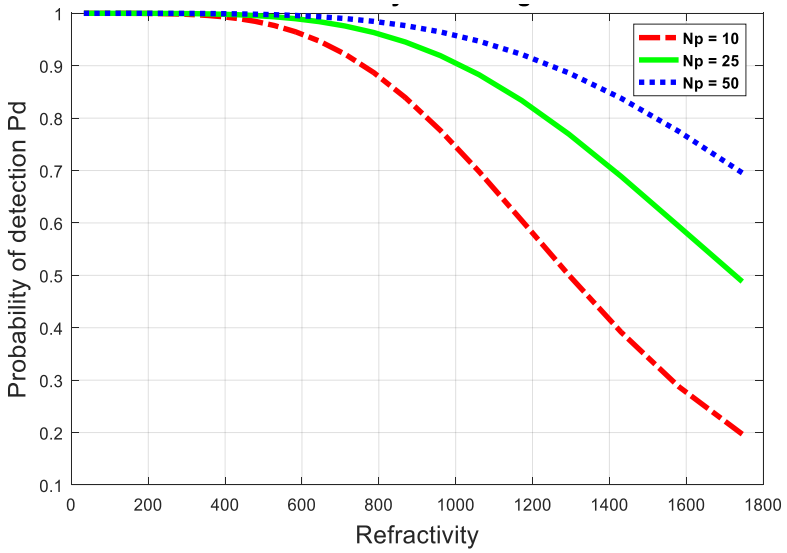

Figure 5.22. Pd vs Refractivity for Swerling Model III.

Attenuation loss is lesser for Swerling model IV only when the refractivity is in small range. If the refractivity increases then the detection capability falls from its maximum value. The probability of detection is almost zero within the range of 800~1200 N-units of refractivity.

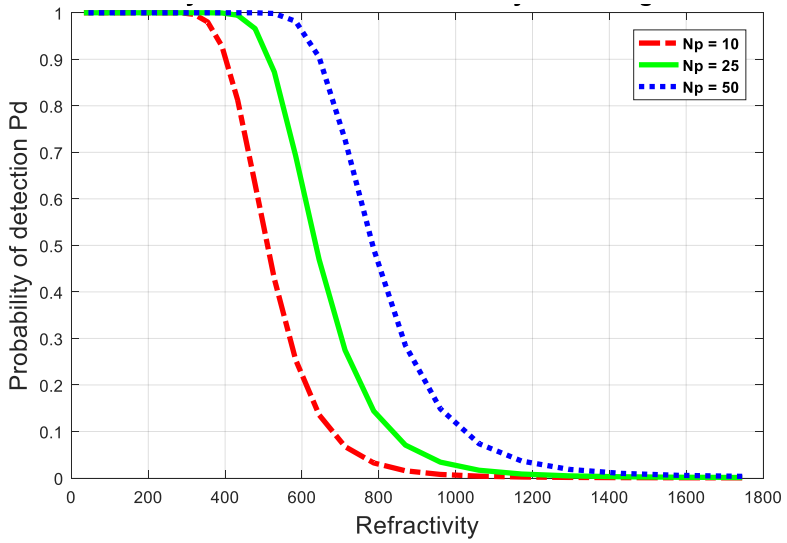

Figure 5.23. Pd vs Refractivity for Swerling Model IV.

After completing the analysis on the simulation of detection capability in terms of reflection coefficient it is seen that the probability of detection decreases for higher values of reflection coefficient for all the target models of Swerling. The maximum detection capability is observed for Swerling model in presence of reflection from earth surface. The behavior of the received signal was also observed for radar system taking consideration the atmosphere of earth. Refraction phenomenon of propagated wave has

a great impact on detection capability of radar. Attenuation due to atmosphere makes radar signal bended. The probability of detection decreases slowly for the increased values of refractivity. All Swerling target models follow this criteria. For different number of pulse the analysis shows different result which are similar to each other. It is observed that for Swerling model II the detection capability is maximum when the number of integrated pulses is higher for various values of refractivity.

5.6. Conclusion

Simulations are done for three different issues in terms of target detection. Various results are taken from the simulations by changing different parameters. All the results are compared with each other and a final solution to improve detection capability is shown in this chapter. Future work is discussed in the next chapter.

CHAPTER SIX

CONCLUSIONS AND FUTURE WORKS

6.1. Conclusions

An analytical approach is presented to evaluate the probability of detection in Radar system. Results are evaluated for a range of system parameters.

In chapter 2, research methodology is discussed regarding related works of RADAR system. The analysis was extended to find the result under different circumstances. Many authors varied different parameters to observe their effects on the radar range by using MATLAB simulation. Doubling the peak power improves SNR only a little whereas doubling the RCS improves SNR a little better. Other radar parameters such as antenna gain variation should be considered to improve SNR or detection range effectively. Integrating a limited number of pulses can significantly enhance the SNR. However, integrating large amount of pulses does not provide any further major improvement in radar performance. To increase the detection capability various conditions were considered by analyzing different publications in this regard.

The first portion of this thesis work presents an analytical method for comparison of probability of detection for various CFAR in RADAR technology. Differences among four Swerling models have been shown and explained in the case of fluctuating target. It is observed that lower constant false alarm rate can give better accuracy in detection. By decreasing the value of CFAR as well as increasing Cell Array can be the better solution where targets are moving.

Second portion of this thesis presents an analytical method for comparison of CFAR loss for various value of gamma function & method of improving detection capability in RADAR technology. Differences among four Swerling model have been simulated in case of fluctuating target. It is observed that lower CFAR loss can give better accuracy in target detection. For probability of detection lower gamma function is also desirable. It has been revealed that decreasing the value of gamma as well as increasing Cell Array can be the better solution where targets are fluctuated.

A method for reduction of side lobes in RADAR technology has been presented in the third part of the thesis. Comparison of various side-lobes has been experimentally demonstrated in the case of analog and digital pulse compression technique. It is seen that the side lobes are different while using different types of pulse compression technique. It has been revealed that side lobes are lower than others for digital pulse compression. In the case of using transversal filter in barker coding, the side lobe tends to zero which results improved signal to noise ratio (SNR) and thus leads to better detection capability.

The performance of RADAR propagated wave with respect to atmospheric attenuation has been presented in this work. There are differences in detection capability for refraction and reflection among four Swerling models and it has been demonstrated in the case of fluctuating target. Observations show that lower value of reflection coefficient can give better performance in target detection. It has also been revealed that changing the parameter refractivity can affect the detection capability. Target tracking will be maximum when the refractivity will be minimum. It also depends on the number of integrated pulse which is transmitted initially. For higher number of integrated pulses the detection capability is better for both the cases of reflection and refraction.

6.2. Future Works

In future analysis, comparison between CFAR loss and Cell array can be an additional version of this research. Higher number of pulses may be analyzed to improve the target detection in RADAR system. Side lobes of target detection can be removed totally by using a new technique besides barker code. In further works, threshold voltage can be adjusted automatically with the change in false alarm rate in RADAR receiver. Relation between CFAR Loss and atmospheric attenuation can also be a new dimension of this research. Attenuation from sea surface of propagated wave can be considered as a future work in this regard. Thus, probability of detection of moving targets can be improved significantly by the implementation of all these methods.

BIBLIOGRAPHY

[1] X. Leng, K. Ji, K. Yang, and H. Zou, "A Bilateral CFAR Algorithm for Ship Detection in SAR Images," *IEEE Geoscience and Remote Sensing Letters*, vol. 12, no. 7, pp. 1536–1540, Jul. 2015.

[2] G. Gigli and G. A. Lampropoulos, "A new maximum likelihood generalized gamma CFAR detector," in *IEEE International Geoscience and Remote Sensing Symposium*, Toronto, Ont., Canada, 2002, vol. 6, pp. 3399–3401.

[3] B. R. Bean, B. A. Cahoon, C. A. Samson, and G. D. Thayer, "A World Atlas of Atmospheric Radio Refractivity (Digest of ESSA Monograph No. 1)," *Radio Science*, vol. 1, no. 9, pp. 1113–1114, Sep. 1966.

[4] A. Aubry, A. De Maio, Bo Jiang, and Shuzhong Zhang, "Ambiguity Function Shaping for Cognitive Radar Via Complex Quartic Optimization," *IEEE Transactions on Signal Processing*, vol. 61, no. 22, pp. 5603–5619, Nov. 2013.

[5] W. An, C. Xie, and X. Yuan, "An Improved Iterative Censoring Scheme for CFAR Ship Detection With SAR Imagery," *IEEE Transactions on Geoscience and Remote Sensing*, vol. 52, no. 8, pp. 4585–4595, Aug. 2014.

[6] M. B. El Mashade, "Analytical performance evaluation of adaptive detection of fluctuating radar targets," *Radioelectronics and Communications Systems*, vol. 56, no. 7, pp. 321–334, Jul. 2013.

[7] F. D. A. Garcia, A. C. F. Rodriguez, G. Fraidenraich, and J. C. S. Santos Filho, "CA-CFAR Detection Performance in Homogeneous Weibull Clutter," *IEEE Geoscience and Remote Sensing Letters*, pp. 1–5, 2018.

[8] Y. Wang, W. Xia, and Z. He, "CFAR Knowledge-Aided Radar Detection With Heterogeneous Samples," *IEEE Signal Processing Letters*, vol. 24, no. 5, pp. 693–697, May 2017.

[9] R. Du, F. Norouzian, E. Marchetti, B. Willetts, M. Gashinova, and M. Cherniakov, "Characterisation of attenuation by sand in low-THz band," in *2017 IEEE Radar Conference (RadarConf)*, Seattle, WA, USA, 2017, pp. 0294–0297.

[10] L. Kong, G. Cui, X. Yang, W. Yi, and B. Wang, "Constant false alarm rate performance prediction for non-independent and non-identically distributed gamma fluctuating targets," *IET Radar, Sonar & Navigation*, vol. 10, no. 5, pp. 992–1000, Jun. 2016.

[11] C. H. Gierull, "Demystifying the Capability of Sublook Correlation Techniques for Vessel Detection in SAR Imagery," *IEEE Transactions on Geoscience and Remote Sensing*, pp. 1–12, 2018.

[12] E. Chaumette, U. Nickel, and P. Larzabal, "Detection and parameter estimation of extended targets using the generalized monopulse estimator," *IEEE Transactions on Aerospace and Electronic Systems*, vol. 48, no. 4, pp. 3389–3417, Oct. 2012.

[13] Tortoli, Guidi, and Atzeni, "Digital vs. SAW matched filter implementation for radar pulse compression," in *Proceedings of IEEE Ultrasonics Symposium ULTSYM-94*, Cannes, France, 1994, pp. 199–202 vol.1.

[14] Yu Gen-miao, Wu Shun-jun, and Luo Yong-jian, “Doppler properties of polyphase pulse compression codes under different side-lobe reduction techniques,” in *2001 CIE International Conference on Radar Proceedings (Cat No.01TH8559)*, Beijing, China, 2001, pp. 524–528.

[15] D. A. Shnidman, “Expanded Swerling target models,” *IEEE Transactions on Aerospace and Electronic Systems*, vol. 39, no. 3, pp. 1059–1069, Jul. 2003.

[16] T. Backes and L. D. Smith, “Improved RCS model for censored Swerling III and IV target models,” in *2013 IEEE Aerospace Conference*, Big Sky, MT, 2013, pp. 1–4.

[17] J. Branson, S. Wooding, and W. N. Dawber, “Modelling of the littoral environment for real-time radar performance assessment,” in *RADAR 2002*, Edinburgh, UK, 2002, pp. 41–46.

[18] B. Bean and G. Thayer, “Models of the Atmospheric Radio Refractive Index,” *Proceedings of the IRE*, vol. 47, no. 5, pp. 740–755, May 1959.

[19] Y. Cui, G. Zhou, J. Yang, and Y. Yamaguchi, “On the Iterative Censoring for Target Detection in SAR Images,” *IEEE Geoscience and Remote Sensing Letters*, vol. 8, no. 4, pp. 641–645, Jul. 2011.

[20] M. B. El Mashade, “Performance Analysis of CFAR Detection of Fluctuating Radar Targets in Nonideal Operating Environments,” *American Journal of Signal Processing*, vol. 2, no. 5, pp. 98–112, Dec. 2012.

[21] B. R. Mahafza, *Radar Systems Analysis and Design Using MATLAB*. CRC Press, 2016.

[22] B. R. Bean, E. J. Dutton, and C. R. P. Laboratory (U.S.), *Radio Meteorology*. Superintendent of Documents, U.S.Government Print.Office, 1966.

[23] X. Wang, M. Yang, S. Zhu, and Y. Lin, “Regionlets for Generic Object Detection,” *IEEE Transactions on Pattern Analysis and Machine Intelligence*, vol. 37, no. 10, pp. 2071–2084, Oct. 2015.

[24] S. L. Durden, “Relating GPM Radar Reflectivity Profile Characteristics to Path-Integrated Attenuation,” *IEEE Transactions on Geoscience and Remote Sensing*, vol. 56, no. 7, pp. 4065–4074, Jul. 2018.

[25] A. Linkova and G. Khlopov, “Retrieval of rain intensity by three-frequency radar sensing,” in *2016 9th International Kharkiv Symposium on Physics and Engineering of Microwaves, Millimeter and Submillimeter Waves (MSMW)*, Kharkiv, Ukraine, 2016, pp. 1–3.

[26] Z. Wang, C. Wang, H. Zhang, F. Wang, F. Jin, and L. Xie, “SAR-based ship detection in sea areas containing small islands,” in *2015 IEEE 5th Asia-Pacific Conference on Synthetic Aperture Radar (APSAR)*, Singapore, Singapore, 2015, pp. 591–595.

[27] J. R. R. Uijlings, K. E. A. van de Sande, T. Gevers, and A. W. M. Smeulders, “Selective Search for Object Recognition,” *International Journal of Computer Vision*, vol. 104, no. 2, pp. 154–171, Sep. 2013.

[28] U. R. O. Nickel, E. Chaumette, and P. Larzabal, “Statistical Performance Prediction of Generalized Monopulse Estimation,” *IEEE Transactions on Aerospace and Electronic Systems*, vol. 47, no. 1, pp. 381–404, Jan. 2011.

[29] A. De Maio, A. Farina, and G. Foglia, “Target fluctuation models and their application to radar performance prediction,” *IEE Proceedings - Radar, Sonar and Navigation*, vol. 151, no. 5, p. 261, 2004.

[30] E. K. Smith and S. Weintraub, “The constants in the equation for atmospheric refractive index at radio frequencies,” *Journal of Research of the National Bureau of Standards*, vol. 50, no. 1, p. 39, Jan. 1953.

[31] B. Bean, “The Radio Refractive Index of Air,” *Proceedings of the IRE*, vol. 50, no. 3, pp. 260–273, Mar. 1962.

[32] E. E. Altshuler, “Tropospheric range-error corrections for the Global Positioning System,” *IEEE Transactions on Antennas and Propagation*, vol. 46, no. 5, pp. 643–649, May 1998.

[33] R. Mamgain, R. Jain, D. Deb, and D. Seshagiri, “Two level CFAR Algorithm for Multiple Target Detection,” in *2018 3rd International Conference for Convergence in Technology (I2CT)*, Pune, 2018, pp. 1–4.

[34] B. Erol, M. G. Amin, B. Boashash, F. Ahmad, and Y. D. Zhang, “Wideband radar based fall motion detection for a generic elderly,” in *2016 50th Asilomar Conference on Signals, Systems and Computers*, Pacific Grove, CA, USA, 2016, pp. 1768–1772.

LIST OF PUBLICATIONS

Published

- **Md. Maynul Islam** and Mohammed Hossam-E-Haider, "Detection Capability and CFAR Loss Under Fluctuating Targets of Different Swerling Model for Various Gamma Parameters in RADAR," *International Journal of Advanced Computer Science and Applications (IJACSA)*, vol. 9, no. 2, pp. 90–93, 2018.

- **Md. Maynul Islam** and Mohammed Hossam-E-Haider, "Analysis of RADAR Performance for Different Fluctuating Target Models of Various False Alarm Rate," *International Journal of Advanced Scientific and Technical Research (IJAST)*, vol. 4, no. 8, pp. 1–6, Aug. 2018.

- **Md. Maynul Islam** and Mohammed Hossam-E-Haider, " *Comparison of Analog and Digital Pulse Compression Technique and Reduction of Side lobes Using Transversal Filter* ", 2nd International Conference on Electrical Engineering and Information & Communication Technology (ICEEICT 2015), Dhaka, 2015

Submitted

- **Md. Maynul Islam** and Mohammed Hossam-E-Haider, "*Performance Analysis of Detection Capability of RADAR in the Case of Atmospheric Attenuation of Propagated RADAR Wave in Different Layers of Earth Atmosphere for Various Target Models"* Journal of the Institute of Navigation.

APPENDIX

MATLAB codes used for simulations

Code for Detection Capability in Presence of False Alarm Rate

SWERLING I

```
clc
clear all
Ns=350;%surface refractivity

hb=12192 % 40kft=12192 m
hs=6000; %target surface altitude in meter
Nb=66.65;
h=0:372:15140;%50 kft =15240 feet
Hb= (hb-hs)/(log(Ns/Nb));
%refractivity=N
k=h-hs
N=Ns*exp(-(h-hs)/Hb)
nfa=10^05;
%np=input('np=')
np=10;
snrbar1=-10:30;

format long
snrbar = 10.^(snrbar1/10);
eps = 0.00000001;
delmax = .00001;
delta =10000.;
%Calculate the threshold Vtfunction [ output_args ] = Untitled(
input_args)

pfa = np * log(2) / nfa
sqrtpfa = sqrt(-log10(pfa));
sqrtnp = sqrt(np);
vt0 = np - sqrtnp + 2.3 * sqrtpfa * (sqrtpfa + sqrtnp - 1.0);
vt = vt0;
while (abs(delta) >= vt0)
igf = gammainc(vt0,np);
%incomplete_gamma(vt0,np);
num = 0.5^(np/nfa) - igf;
temp = (np-1) * log(vt0+eps) - vt0 - factor(np-1);
deno = exp(temp);
vt = vt0 + (num./(deno+eps));
delta = abs(vt - vt0) * 10000.0;
vt0 = vt;
end

if (np == 1)
temp = -vt ./ (1.0 + snrbar)

pd = exp(temp);
%return
end
```

```
vt=vt(1);
temp1 = 1.0 + np * snrbar;
temp2 = 1.0./(np *snrbar);
temp = 1.0 + temp2;
val1 = temp.^(np-1.);

igf1 = gammainc(vt,np-1);%incomplete_gamma(vt(1),np1-1);
c = vt./temp;
igf2 =gammainc(c,(np-1));% incomplete_gamma(c,(np1-1));
pd = 1.0 - igf1 + (val1.* igf2 .* exp(-vt(1)./temp1));


plot(snrbar1,pd)
xlabel('SNR dB')
ylabel('Probability of Detection')

% hold on
M=0:40;% Cell array
cfar=-(5./M)*log10(pfa);

hb=12192 % 40kft=12192 m
hs=6000; %target surface altitude in meter
Nb=66.65;
h=0:372:15140;%50 kft =15240 feet
Hb= (hb-hs)/(log(Ns/Nb));
%refractivity=N
k=h-hs
N=Ns*exp(-(h-hs)/Hb)
nfa=10^05
%np=input('np=')
np=25;
snrbar1=-10:30;

format long
snrbar = 10.^(snrbar1/10);
eps = 0.00000001;
delmax = .00001;
delta =10000.;
%Calculate the threshold Vtfunction [ output_args ] = Untitled(
input_args )
%UNTITLED Summary of this function goes here
%Detailed explanation goes here
pfa = np * log(2) / nfa
sqrtpfa = sqrt(-log10(pfa));
sqrtnp = sqrt(np);
vt0 = np - sqrtnp + 2.3 * sqrtpfa * (sqrtpfa + sqrtnp - 1.0);
vt = vt0;
while (abs(delta) >= vt0)
igf = gammainc(vt0,np);
%incomplete_gamma(vt0,np);
num = 0.5^(np/nfa) - igf;
temp = (np-1) * log(vt0+eps) - vt0 - factor(np-1);
deno = exp(temp);
vt = vt0 + (num./(deno+eps));
delta = abs(vt - vt0) * 10000.0;
vt0 = vt;
end

if (np == 1)
temp = -vt ./ (1.0 + snrbar)
pd = exp(temp);
```

```
%return
end
vt=vt(1);
temp1 = 1.0 + np * snrbar;
temp2 = 1.0./(np *snrbar);
temp = 1.0 + temp2;
val1 = temp.^(np-1.);

igf1 = gammainc(vt,np-1);%incomplete_gamma(vt(1),np1-1);
c = vt./temp;
igf2 =gammainc(c,(np-1));% incomplete_gamma(c,(np1-1));
pd = 1.0 - igf1 + (val1.* igf2 .* exp(-vt(1)./temp1));


%plot(snrbar1,pd)
xlabel('SNR dB')
ylabel('Probability of Detection')

% hold on
M=0:40;% Cell array
cfar=-(5./M)*log10(pfa);

hold on
clc
clear all
Ns=350;%surface refractivity

hb=12192 % 40kft=12192 m
hs=6000; %target surface altitude in meter
Nb=66.65;
h=0:372:15140;%50 kft =15240 feet
Hb= (hb-hs)/(log(Ns/Nb));
%refractivity=N
k=h-hs
N=Ns*exp(-(h-hs)/Hb)
nfa=10^05
%np=input('np=')
np=50;
snrbar1=-10:30;

format long
snrbar = 10.^(snrbar1/10);
eps = 0.00000001;
delmax = .00001;
delta =10000.;
%Calculate the threshold Vtfunction [ output_args ] = Untitled(
input_args )
%UNTITLED Summary of this function goes here
%Detailed explanation goes here
pfa = np * log(2) / nfa
sqrtpfa = sqrt(-log10(pfa));
sqrtnp = sqrt(np);
vt0 = np - sqrtnp + 2.3 * sqrtpfa * (sqrtpfa + sqrtnp - 1.0);
vt = vt0;
while (abs(delta) >= vt0)
igf = gammainc(vt0,np);
%incomplete_gamma(vt0,np);
num = 0.5^(np/nfa) - igf;
temp = (np-1) * log(vt0+eps) - vt0 - factor(np-1);
deno = exp(temp);
vt = vt0 + (num./(deno+eps));
```

```
delta = abs(vt - vt0) * 10000.0;
vt0 = vt;
end

if (np == 1)
temp = -vt ./ (1.0 + snrbar)

pd = exp(temp);
%return
end
vt=vt(1);
temp1 = 1.0 + np * snrbar;
temp2 = 1.0./(np *snrbar);
temp = 1.0 + temp2;
val1 = temp.^(np-1.);

igf1 = gammainc(vt,np-1);%incomplete_gamma(vt(1),np1-1);
c = vt./temp;
igf2 =gammainc(c,(np-1));% incomplete_gamma(c,(np1-1));
pd = 1.0 - igf1 + (val1.* igf2 .* exp(-vt(1)./temp1));


plot(snrbar1,pd)
xlabel('SNR dB')
ylabel('Probability of Detection')

% hold on
M=0:40;% Cell array
cfar=-(5./M)*log10(pfa);
%plot(c,pd,'b')
%plot(igf2,cfar,'b')
plot(N,pd,'b')
ylabel('CFAR Loss(dB)')
% xlabel('Probability of Detection')
%ylabel('CFAR')
 xlabel('Gamma Function')
% ylabel('Probability of Detection')
title('Pd vs SNR)


xlabel('SNR dB')
ylabel('Probability of Detection')
```

SWERLING II

```
clc
clear all
close all
nfa=10^05;
np=10;

snrbar1=-10:30;
format long
snrbar = 10.^(snrbar1/10);
eps = 0.00000001;
delmax = .00001;
delta =10000.;
% Calculate the threshold Vt
pfa = np * log(2) / nfa;
sqrtpfa = sqrt(-log10(pfa));
```

```
sqrtnp = sqrt(np);
vt0 = np - sqrtnp + 2.3 * sqrtpfa * (sqrtpfa + sqrtnp - 1.0);
vt= vt0;

while (abs(delta) >= vt0)
igf = gammainc(vt0,np)% igf = incomplete_gamma(vt0,np)
num = 0.5^(np/nfa) - igf;
temp = (np-1) * log(vt0+eps) - vt0 - factor(np-1);
deno = exp(temp);
vt = vt + (num./(deno+eps));
delta = abs(vt - vt0) * 10000.0;
vt0 = vt;
end
vt=vt(1);
if (np <= 50)
temp = vt./(1+snrbar);
c= gammainc(temp,np);%incomplete_gamma(temp,np);
pd = 1.0 - c;
%return
else
temp1 = snrbar + 1.0;
omegabar = sqrt(np) * temp1;
c3 = -1.0 / sqrt(np);
c4 = 1/(4*np);
c6 = (c3 * c3) /2.0;
V = (vt - (np * temp1)) / omegabar;
Vsqr = V *V;
val1 = exp(-Vsqr / 2.0) / sqrt( 2.0 * pi);
val2 = c3 * (V^2 -1.0) + c4 * V * (3.0 - V^2) -(c6 * V * (V^4 - 10. *
V^2 + 15.0));
q = 0.5 * erfc (V/sqrt(2.0));
pd = q - val1 * val2
end
%plot(snrbar1,pd)
xlabel('SNR dB')
ylabel('Probability of Detection')


M=0:40;% Cell array
cfar=-(5./M)*log10(pfa);
plot(c,cfar,'r')
%xlabel('Probability of Detection')
%ylabel('CFAR')
%plot(snrbar1,cfar,'r')

xlabel('Gamma Function')
ylabel('CFAR')
title('CFAR vs Gamma Function for Swerling 2')


hold on
clc
clear all
nfa=10^5;
np=25;

snrbar1=-10:30;
format long
snrbar = 10.^(snrbar1/10);
eps = 0.00000001;
delmax = .00001;
```

```
delta =10000.;
% Calculate the threshold Vt
pfa = np * log(2) / nfa;
sqrtpfa = sqrt(-log10(pfa));
sqrtnp = sqrt(np);
vt0 = np - sqrtnp + 2.3 * sqrtpfa * (sqrtpfa + sqrtnp - 1.0);
vt= vt0;

while (abs(delta) >= vt0)
igf = gammainc(vt0,np)% igf = incomplete_gamma(vt0,np)
num = 0.5^(np/nfa) - igf;
temp = (np-1) * log(vt0+eps) - vt0 - factor(np-1);
deno = exp(temp);
vt = vt + (num./(deno+eps));
delta = abs(vt - vt0) * 10000.0;
vt0 = vt;
end
vt=vt(1);
if (np <= 50)
temp = vt./(1+snrbar);
c= gammainc(temp,np);%incomplete_gamma(temp,np);
pd = 1.0 - c;
% return
else
temp1 = snrbar + 1.0;
omegabar = sqrt(np) * temp1;
c3 = -1.0 / sqrt(np);
c4 = 1/(4*np);
c6 = (c3 * c3) /2.0;
V = (vt - (np * temp1)) / omegabar;
Vsqr = V *V;
val1 = exp(-Vsqr / 2.0) / sqrt( 2.0 * pi);
val2 = c3 * (V^2 -1.0) + c4 * V * (3.0 - V^2) -(c6 * V * (V^4 - 10. *
V^2 + 15.0));
q = 0.5 * erfc (V/sqrt(2.0));
pd = q - val1 * val2
end
%plot(snrbar1,pd)
xlabel('SNR dB')
ylabel('Probability of Detection')

% hold on
M=0:40;% Cell array
cfar=-(5./M)*log10(pfa);
%plot(pd,cfar)
%xlabel('Probability of Detection')
%ylabel('CFAR')
plot(c,cfar,'g')
xlabel('Gamma Function')
ylabel('CFAR')
title('CFAR vs Gamma Function for Swerling 2')

hold on
clc
clear all
nfa=10^5;
np=50;

snrbar1=-10:30;
format long
snrbar = 10.^(snrbar1/10);
```

```
eps = 0.00000001;
delmax = .00001;
delta =10000.;
% Calculate the threshold Vt
pfa = np * log(2) / nfa
sqrtpfa = sqrt(-log10(pfa));
sqrtnp = sqrt(np);
vt0 = np - sqrtnp + 2.3 * sqrtpfa * (sqrtpfa + sqrtnp - 1.0);
vt= vt0;

while (abs(delta) >= vt0)
igf = gammainc(vt0,np)% igf = incomplete_gamma(vt0,np)
num = 0.5^(np/nfa) - igf;
temp = (np-1) * log(vt0+eps) - vt0 - factor(np-1);
deno = exp(temp);
vt = vt + (num./(deno+eps));
delta = abs(vt - vt0) * 10000.0;
vt0 = vt;
end
vt=vt(1);
if (np <= 50)
temp = vt./(1+snrbar);
c= gammainc(temp,np);%incomplete_gamma(temp,np);
pd = 1.0 - c;
% return
else
temp1 = snrbar + 1.0;
omegabar = sqrt(np) * temp1;
c3 = -1.0 / sqrt(np);
c4 = 1/(4*np);
c6 = (c3 * c3) /2.0;
V = (vt - (np * temp1)) / omegabar;
Vsqr = V *V;
val1 = exp(-Vsqr / 2.0) / sqrt( 2.0 * pi);
val2 = c3 * (V^2 -1.0) + c4 * V * (3.0 - V^2) -(c6 * V * (V^4 - 10. *
V^2 + 15.0));
q = 0.5 * erfc (V/sqrt(2.0));
pd = q - val1 * val2
end
%plot(snrbar1,pd)
xlabel('SNR dB')
ylabel('Probability of Detection')

% hold on
M=0:40;% Cell array
cfar=-(5./M)*log10(pfa);
plot(c,cfar,'b')

title('Probability of Detection vs SNR for Swerling 2')
```

SWERLING III

```
clc
clear all
nfa=10^5;
np=10;

snrbar1=0:40;
format long
snrbar = 10.^(snrbar1/10);
```

```
eps = 0.00000001;
delmax = .00001;
delta =10000.;
% Calculate the threshold Vt
pfa = np * log(2) / nfa;
sqrtpfa = sqrt(-log10(pfa));
sqrtnp = sqrt(np);
vt0 = np - sqrtnp + 2.3 * sqrtpfa * (sqrtpfa + sqrtnp - 1.0);
vt = vt0;
while (abs(delta) >= vt0)
igf = gammainc(vt0,np);%incomplete_gamma(vt0,np);
num = 0.5^(np/nfa) - igf;
temp = (np-1) * log(vt0+eps) - vt0 - factor(np-1);
deno = exp(temp);
vt = vt0 + (num./(deno+eps));
delta = abs(vt - vt0) * 10000.0;
vt0 = vt;
end
vt=vt(1);
temp1 = vt./(1+0.5*np*snrbar);
temp2 = 1+ (2./(np*snrbar));
temp3 = 2.0 * (np - 2.0)./ (np * snrbar);
ko = exp(-temp1).* temp2.^(np-2.).* (1.0 + temp1 - temp3);
if (np <= 2)
pd = ko;
% return
else
temp4 = vt.^(np-1.).* exp(-vt)./ (temp1*exp(factorial(np-2.)));
temp5 = vt./(1.0 + 2.0./ (np *snrbar));
pd = temp4 + 1.0 - gammainc(vt,np-1.) + ko.*gammainc(temp5,np-1.);
end

%plot(snrbar1,pd)
xlabel('SNR dB')
ylabel('Probability of Detection')
% hold on
M=0:40;% Cell array
cfar=-(5./M)*log10(pfa);
%plot(pd,cfar)
% xlabel('Probability of Detection')
% ylabel('CFAR')

%title('CFAR vs Pd for Swerling 3')
%plot(cfar,temp1,'r')
plot(temp1,cfar,'r')

xlabel('Gamma Function')
ylabel('CFAR')
title('CFAR vs Gamma Function for Swerling 3')


hold on
clc
clear all
nfa=10^5;
np=25;

snrbar1=0:40;
format long
snrbar = 10.^(snrbar1/10);
eps = 0.00000001;
```

```
delmax = .00001;
delta =10000.;
% Calculate the threshold Vt
pfa = np * log(2) / nfa;
sqrtpfa = sqrt(-log10(pfa));
sqrtnp = sqrt(np);
vt0 = np - sqrtnp + 2.3 * sqrtpfa * (sqrtpfa + sqrtnp - 1.0);
vt = vt0;
while (abs(delta) >= vt0)
igf = gammainc(vt0,np);%incomplete_gamma(vt0,np);
num = 0.5^(np/nfa) - igf;
temp = (np-1) * log(vt0+eps) - vt0 - factor(np-1);
deno = exp(temp);
vt = vt0 + (num./(deno+eps));
delta = abs(vt - vt0) * 10000.0;
vt0 = vt;
end
vt=vt(1);
temp1 = vt./(1+0.5*np*snrbar);
temp2 = 1+ (2./(np*snrbar));
temp3 = 2.0 * (np - 2.0)./ (np * snrbar);
ko = exp(-temp1).* temp2.^(np-2.).* (1.0 + temp1 - temp3);
if (np <= 2)
pd = ko;
% return
else
temp4 = vt.^(np-1.).* exp(-vt)./ (temp1*exp(factorial(np-2.)));
temp5 = vt./(1.0 + 2.0./ (np *snrbar));
pd = temp4 + 1.0 - gammainc(vt,np-1.) + ko.*gammainc(temp5,np-1.);
end

%plot(snrbar1,pd)
xlabel('SNR dB')
ylabel('Probability of Detection')
% hold on
M=0:40;% Cell array
cfar=-(5./M)*log10(pfa);
%plot(pd,cfar)
% xlabel('Probability of Detection')
% ylabel('CFAR')

%title('CFAR vs Pd for Swerling 3')

% plot(cfar,temp1,'g')
plot(temp1,cfar,'g')

xlabel('Gamma Function')
ylabel('CFAR')
title('CFAR vs Gamma Function for Swerling 3')

hold on
clc
clear all
nfa=10^5;
np=50;

snrbar1=0:40;
format long
snrbar = 10.^(snrbar1/10);
eps = 0.00000001;
delmax = .00001;
```

```
delta =10000.;
% Calculate the threshold Vt
pfa = np * log(2) / nfa;
sqrtpfa = sqrt(-log10(pfa));
sqrtnp = sqrt(np);
vt0 = np - sqrtnp + 2.3 * sqrtpfa * (sqrtpfa + sqrtnp - 1.0);
vt = vt0;
while (abs(delta) >= vt0)
igf = gammainc(vt0,np);%incomplete_gamma(vt0,np);
num = 0.5^(np/nfa) - igf;
temp = (np-1) * log(vt0+eps) - vt0 - factor(np-1);
deno = exp(temp);
vt = vt0 + (num./(deno+eps));
delta = abs(vt - vt0) * 10000.0;
vt0 = vt;
end
vt=vt(1);
temp1 = vt./(1+0.5*np*snrbar);
temp2 = 1+ (2./(np*snrbar));
temp3 = 2.0 * (np - 2.0)./ (np * snrbar);
ko = exp(-temp1).* temp2.^(np-2.).* (1.0 + temp1 - temp3);
if (np <= 2)
pd = ko;
% return
else
temp4 = vt.^(np-1.).* exp(-vt)./ (temp1*exp(factorial(np-2.)));
temp5 = vt./(1.0 + 2.0./ (np *snrbar));
pd = temp4 + 1.0 - gammainc(vt,np-1.) + ko.*gammainc(temp5,np-1.);
end


%plot(snrbar1,pd)
xlabel('SNR dB')
ylabel('Probability of Detection')
% hold on
M=0:40;% Cell array
cfar=-(5./M)*log10(pfa);
%plot(pd,cfar)
% xlabel('Probability of Detection')
% ylabel('CFAR')

%title('CFAR vs Pd for Swerling 3')

% plot(cfar,temp1,'b')
plot(temp1,cfar,'b')

xlabel('Gamma Function')
ylabel('CFAR Loss(dB)')
title('CFAR Loss vs Gamma Function for Swerling 3')
% xlabel('Gamma Function')
% ylabel('Probability of Detection')
% title('Probability of Detection vs Gamma Function for Swerling 3')
```

SWERLING IV

```
clc
clear all
nfa=10^5;
np=10;
M=0:40; % Cell array
```

```
snrbar1=-10:30;

% This function is used to calculate the probability of
%  Swerling 4 targets.
format long
snrbar = 10.^(snrbar1/10);
eps = 0.00000001;
delmax = .00001;
delta =10000;
% Calculate the threshold Vt
pfa = np * log(2) / nfa
cfar=-(5./M)*log10(pfa);
sqrtpfa = sqrt(-log10(pfa));
sqrtnp = sqrt(np);
vt0 = np - sqrtnp + 2.3 * sqrtpfa * (sqrtpfa + sqrtnp - 1.0);
vt = vt0;
while (abs(delta) >= vt0)
igf = gammainc(vt0,np); %incomplete_gamma(vt0,np);
num = 0.5^(np/nfa) - igf;
temp = (np-1) * log(vt0+eps) - vt0 - factor(np-1);
deno = exp(temp);
vt = vt0 + (num./(deno+eps));
delta = abs(vt - vt0) * 10000.0;
vt0 = vt;
end
vt=vt(1);
h8 = snrbar/2.0;
beta = 1.0 + h8;
beta2 = 2.* beta.^2 - 1;
beta3 = 2.0 * beta.^3;
if (np >= 50)
temp1 = 2*beta.^4;
omegabar = sqrt(np * beta2);
c3 = (beta3 - 1)./(3.*(beta2).*omegabar);
c4 = (temp1 - 1.0)/(4.*np.*(beta2).^2);
c6 = (c3.*c3)/2.0;

V = (vt - np*(1.0 + snrbar)) / omegabar;
Vsqr =  V*V;
exp(-Vsqr / 2.0); % ???? have to solve.
val1 = exp(-Vsqr / 2.0)/ sqrt( 2.0 * pi);
val2 = (c3*(V^2 -1.0)) + (c4 * V *(3.0 - V^2)) - (c6*V*(V^4 - (10*
V^2) + 15.0));

q = 0.5 * erfc(V/sqrt(2.0));
pd = q - (val1 * val2);
% return
else

snr = 1.0;
gamma0 = gammainc((vt./beta),np);%incomplete_gamma(vt./beta,np);
d11=(exp(vt./beta));
%d12=exp(factor(np))
a1 = ((vt./beta).^np)./(factorial(np).*d11);
sum = gamma0;
for i = 1:1:np
temp1 = 1;
if (i == 1)
ai = a1;
```

```
else
ai = (vt./ beta).* a1 / (np + i -1);
end
a1 = ai;
gammai = gamma0 - ai;
gamma0 = gammai;
a1 = ai;
for ii = 1:1:i
temp1 = temp1 * (np + 1 - ii);
end
term = (snrbar /2.0).^i.* gammai.*temp1 / factorial(i);
sum = sum + term;
end
pd = 1.- sum./ beta.^np;
end
pd = max(pd,0.);

%plot(snrbar1,pd)
xlabel('SNR dB')
ylabel('Probability of Detection')
hold on
%plot(cfar,M)
xlabel('Cell array')
ylabel('CFAR')

M=0:40;% Cell array
cfar=-(5./M)*log10(pfa);
%plot(cfar,pd)
plot(gamma0,cfar,'r')
%plot(gamma0,pd,'r')
ylabel('Probability of Detection')
xlabel('CFAR')

title('CFAR vs Pd for Swerling 4')
%f=fit(cfar',pd','poly3')

hold on
clc
clear all
nfa=10^5;
np=20;
M=0:40; % Cell array
snrbar1=-10:30;

% This function is used to calculate the probability of
%  Swerling 4 targets.
format long
snrbar = 10.^(snrbar1/10);
eps = 0.00000001;
delmax = .00001;
delta =10000;
% Calculate the threshold Vt
pfa = np * log(2) / nfa
cfar=-(5./M)*log10(pfa);
sqrtpfa = sqrt(-log10(pfa));
sqrtnp = sqrt(np);
vt0 = np - sqrtnp + 2.3 * sqrtpfa * (sqrtpfa + sqrtnp - 1.0);
vt = vt0;
while (abs(delta) >= vt0)
igf = gammainc(vt0,np); %incomplete_gamma(vt0,np);
num = 0.5^(np/nfa) - igf;
```

```
temp = (np-1) * log(vt0+eps) - vt0 - factor(np-1);
deno = exp(temp);
vt = vt0 + (num./(deno+eps));
delta = abs(vt - vt0) * 10000.0;
vt0 = vt;
end
vt=vt(1);
h8 = snrbar/2.0;
beta = 1.0 + h8;
beta2 = 2.* beta.^2 - 1;
beta3 = 2.0 * beta.^3;
if (np >= 50)
temp1 = 2*beta.^4;
omegabar = sqrt(np * beta2);
c3 = (beta3 - 1)./(3.*(beta2).*omegabar);
c4 = (temp1 - 1.0)/(4.*np.*(beta2).^2);
c6 = (c3.*c3)/2.0;

V = (vt - np*(1.0 + snrbar)) / omegabar;
Vsqr =  V*V;
exp(-Vsqr / 2.0); % ???? have to solve.
val1 = exp(-Vsqr / 2.0)/ sqrt( 2.0 * pi);
val2 = (c3*(V^2 -1.0)) + (c4 * V *(3.0 - V^2)) - (c6*V*(V^4 - (10*
V^2) + 15.0));

q = 0.5 * erfc(V/sqrt(2.0));
pd = q - (val1 * val2);
% return
else

snr = 1.0;
gamma0 = gammainc((vt./beta),np);%incomplete_gamma(vt./beta,np);
d11=(exp(vt./beta));
%d12=exp(factor(np))
a1 = ((vt./beta).^np)./(factorial(np).*d11);
sum = gamma0;
for i = 1:1:np
temp1 = 1;
if (i == 1)
ai = a1;



else
ai = (vt./ beta).* a1 / (np + i -1);
end
a1 = ai;
gammai = gamma0 - ai;
gamma0 = gammai;
a1 = ai;
for ii = 1:1:i
temp1 = temp1 * (np + 1 - ii);
end
term = (snrbar /2.0).^i.* gammai.*temp1 / factorial(i);
sum = sum + term;
end
pd = 1.- sum./ beta.^np;
end
pd = max(pd,0.);

%plot(snrbar1,pd)
xlabel('SNR dB')
```

```
ylabel('Probability of Detection')
hold on
%plot(cfar,M)
xlabel('Cell array')
ylabel('CFAR')

M=0:40;% Cell array
cfar=-(5./M)*log10(pfa);
%plot(cfar,pd)
plot(gamma0,cfar,'g')
%plot(gamma0,pd,'g')
ylabel('Probability of Detection')
xlabel('CFAR')

title('CFAR vs Pd for Swerling 4')
%f=fit(cfar',pd','poly3')


hold on
clc
clear all
nfa=10^5;
np=40;
M=0:40; % Cell array
snrbar1=-10:30;

% This function is used to calculate the probability of
%  Swerling 4 targets.
format long
snrbar = 10.^(snrbar1/10);
eps = 0.00000001;
delmax = .00001;
delta =10000;
% Calculate the threshold Vt
pfa = np * log(2) / nfa
cfar=-(5./M)*log10(pfa);
sqrtpfa = sqrt(-log10(pfa));
sqrtnp = sqrt(np);
vt0 = np - sqrtnp + 2.3 * sqrtpfa * (sqrtpfa + sqrtnp - 1.0);
vt = vt0;
while (abs(delta) >= vt0)
igf = gammainc(vt0,np); %incomplete_gamma(vt0,np);
num = 0.5^(np/nfa) - igf;
temp = (np-1) * log(vt0+eps) - vt0 - factor(np-1);
deno = exp(temp);
vt = vt0 + (num./(deno+eps));
delta = abs(vt - vt0) * 10000.0;
vt0 = vt;
end
vt=vt(1);
h8 = snrbar/2.0;
beta = 1.0 + h8;
beta2 = 2.* beta.^2 - 1;
beta3 = 2.0 * beta.^3;
if (np >= 50)
temp1 = 2*beta.^4;
omegabar = sqrt(np * beta2);
c3 = (beta3 - 1)./(3.*(beta2).*omegabar);
c4 = (temp1 - 1.0)/(4.*np.*(beta2).^2);
c6 = (c3.*c3)/2.0;
```

```
V = (vt - np*(1.0 + snrbar)) / omegabar;
Vsqr =  V*V;
exp(-Vsqr / 2.0); % ???? have to solve.
val1 = exp(-Vsqr / 2.0)/ sqrt( 2.0 * pi);
val2 = (c3*(V^2 -1.0)) + (c4 * V *(3.0 - V^2)) - (c6*V*(V^4 - (10*
V^2) + 15.0));

q = 0.5 * erfc(V/sqrt(2.0));
pd = q - (val1 * val2);
% return
else

snr = 1.0;
gamma0 = gammainc((vt./beta),np);%incomplete_gamma(vt./beta,np);
d11=(exp(vt./beta));
%d12=exp(factor(np))
a1 = ((vt./beta).^np)./(factorial(np).*d11);
sum = gamma0;
for i = 1:1:np
temp1 = 1;
if (i == 1)
ai = a1;


else
ai = (vt./ beta).* a1 / (np + i -1);
end
a1 = ai;
gammai = gamma0 - ai;
gamma0 = gammai;
a1 = ai;
for ii = 1:1:i
temp1 = temp1 * (np + 1 - ii);
end
term = (snrbar /2.0).^i.* gammai.*temp1 / factorial(i);
sum = sum + term;
end
pd = 1.- sum./ beta.^np;
end
pd = max(pd,0.);

%plot(snrbar1,pd)
xlabel('SNR dB')
ylabel('Probability of Detection')
hold on
%plot(cfar,M)
xlabel('Cell array')
ylabel('CFAR')

M=0:40;% Cell array
cfar=-(5./M)*log10(pfa);
%plot(cfar,pd)
plot(gamma0,cfar,'b')
%plot(gamma0,pd,'b')
% ylabel('Probability of Detection')
% xlabel('CFAR')
%
% title('CFAR vs Pd for Swerling 4')
%f=fit(cfar',pd','poly3')
ylabel('CFAR Loss(dB)')
xlabel('Gamma Function')
```

```
title(''Probability of Detection vs SNR for Swerling 4')
```

Code for Detection Capability and CFAR Loss vs Threshold Voltage

SWERLING I

```
clc
clear all
nfa=10^05;
%np=input('np=')
np=10;
snrbar1=-10:30;

format long
snrbar = 10.^(snrbar1/10);
eps = 0.00000001;
delmax = .00001;
delta =10000.;
%Calculate the threshold Vtfunction [ output_args ] = Untitled(
input_args)
%UNTITLED Summary of this function goes here
%Detailed explanation goes here
pfa = np * log(2) / nfa
sqrtpfa = sqrt(-log10(pfa));
sqrtnp = sqrt(np);
vt0 = np - sqrtnp + 2.3 * sqrtpfa * (sqrtpfa + sqrtnp - 1.0);
vt = vt0;
while (abs(delta) >= vt0)
igf = gammainc(vt0,np);
%incomplete_gamma(vt0,np);
num = 0.5^(np/nfa) - igf;
temp = (np-1) * log(vt0+eps) - vt0 - factor(np-1);
deno = exp(temp);
vt = vt0 + (num./(deno+eps));
delta = abs(vt - vt0) * 10000.0;
vt0 = vt;
end

if (np == 1)
temp = -vt ./ (1.0 + snrbar)


pd = exp(temp);
%return
end
vt=vt(1);
temp1 = 1.0 + np * snrbar;
temp2 = 1.0./(np *snrbar);
temp = 1.0 + temp2;
val1 = temp.^(np-1.);

igf1 = gammainc(vt,np-1);%incomplete_gamma(vt(1),np1-1);
c = vt./temp;
igf2 =gammainc(c,(np-1));% incomplete_gamma(c,(np1-1));
pd = 1.0 - igf1 + (val1.* igf2 .* exp(-vt(1)./temp1));
```

```
%plot(snrbar1,pd)
xlabel('SNR dB')
ylabel('Probability of Detection')

% hold on
M=0:40;% Cell array
cfar=-(5./M)*log10(pfa);
% plot(c,pd,'r')
plot(igf2,cfar,'r')
xlabel('Gamma Parameter')
ylabel('CFAR')
%xlabel('Probability of Detection')
%ylabel('CFAR')

title('CFAR vs Gamma Parameter for Swerling 1')

%title('CFAR vs Pd for Swerling 1')

hold on
clc
clear all
nfa=10^05
%np=input('np=')
np=25;
snrbar1=-10:30;

format long
snrbar = 10.^(snrbar1/10);
eps = 0.00000001;
delmax = .00001;
delta =10000.;
%Calculate the threshold Vtfunction [ output_args ] = Untitled(
input_args )
%UNTITLED Summary of this function goes here
%Detailed explanation goes here
pfa = np * log(2) / nfa
sqrtpfa = sqrt(-log10(pfa));
sqrtnp = sqrt(np);
vt0 = np - sqrtnp + 2.3 * sqrtpfa * (sqrtpfa + sqrtnp - 1.0);
vt = vt0;
while (abs(delta) >= vt0)
igf = gammainc(vt0,np);
%incomplete_gamma(vt0,np);
num = 0.5^(np/nfa) - igf;
temp = (np-1) * log(vt0+eps) - vt0 - factor(np-1);
deno = exp(temp);
vt = vt0 + (num./(deno+eps));
delta = abs(vt - vt0) * 10000.0;
vt0 = vt;
end

if (np == 1)
temp = -vt ./ (1.0 + snrbar)


pd = exp(temp);
%return
end
vt=vt(1);
```

```
temp1 = 1.0 + np * snrbar;
temp2 = 1.0./(np *snrbar);
temp = 1.0 + temp2;
val1 = temp.^(np-1.);

igf1 = gammainc(vt,np-1);%incomplete_gamma(vt(1),np1-1);
c = vt./temp;
igf2 =gammainc(c,(np-1));% incomplete_gamma(c,(np1-1));
pd = 1.0 - igf1 + (val1.* igf2 .* exp(-vt(1)./temp1));


%plot(snrbar1,pd)
xlabel('SNR dB')
ylabel('Probability of Detection')

% hold on
M=0:40;% Cell array
cfar=-(5./M)*log10(pfa);
% plot(c,pd,'g')
plot(igf2,cfar,'g')
xlabel('Gamma Parameter')
ylabel('CFAR')
%xlabel('Probability of Detection')
%ylabel('CFAR')

title('CFAR vs Gamma Parameter for Swerling 1')

%title('CFAR vs Pd for Swerling 1')



hold on
clc
clear all
nfa=10^05
%np=input('np=')
np=50;
snrbar1=-10:30;

format long
snrbar = 10.^(snrbar1/10);
eps = 0.00000001;
delmax = .00001;
delta =10000.;
%Calculate the threshold Vtfunction [ output_args ] = Untitled(
input_args )
%UNTITLED Summary of this function goes here
%Detailed explanation goes here
pfa = np * log(2) / nfa
sqrtpfa = sqrt(-log10(pfa));
sqrtnp = sqrt(np);
vt0 = np - sqrtnp + 2.3 * sqrtpfa * (sqrtpfa + sqrtnp - 1.0);
vt = vt0;
while (abs(delta) >= vt0)
igf = gammainc(vt0,np);
%incomplete_gamma(vt0,np);
num = 0.5^(np/nfa) - igf;
temp = (np-1) * log(vt0+eps) - vt0 - factor(np-1);
deno = exp(temp);
vt = vt0 + (num./(deno+eps));
```

```
delta = abs(vt - vt0) * 10000.0;
vt0 = vt;
end

if (np == 1)
temp = -vt ./ (1.0 + snrbar)


pd = exp(temp);
%return
end
vt=vt(1);
temp1 = 1.0 + np * snrbar;
temp2 = 1.0./(np *snrbar);
temp = 1.0 + temp2;
val1 = temp.^(np-1.);

igf1 = gammainc(vt,np-1);%incomplete_gamma(vt(1),np1-1);
c = vt./temp;
igf2 =gammainc(c,(np-1));% incomplete_gamma(c,(np1-1));
pd = 1.0 - igf1 + (val1.* igf2 .* exp(-vt(1)./temp1));


%plot(snrbar1,pd)
xlabel('SNR dB')
ylabel('Probability of Detection')

% hold on
M=0:40;% Cell array
cfar=-(5./M)*log10(pfa);
%plot(c,pd,'b')
plot(igf2,cfar,'b')
ylabel('CFAR Loss(dB)')
% xlabel('Probability of Detection')
%ylabel('CFAR')
 xlabel('Gamma Function')
% ylabel('Probability of Detection')
% title('Probability of Detection vs Gamma Function for Swerling 1')

% title('CFAR Loss vs Pd for Swerling 1')
title('CFAR Loss vs Gamma Function for Swerling 1')
```

SWERLING II

```
clc
clear all
close all
nfa=10^05;
np=10;

snrbar1=-10:30;
format long
snrbar = 10.^(snrbar1/10);
eps = 0.00000001;
delmax = .00001;
delta =10000.;
% Calculate the threshold Vt
pfa = np * log(2) / nfa;
sqrtpfa = sqrt(-log10(pfa));
```

```
sqrtnp = sqrt(np);
vt0 = np - sqrtnp + 2.3 * sqrtpfa * (sqrtpfa + sqrtnp - 1.0);
vt= vt0;

while (abs(delta) >= vt0)
igf = gammainc(vt0,np)% igf = incomplete_gamma(vt0,np)
num = 0.5^(np/nfa) - igf;
temp = (np-1) * log(vt0+eps) - vt0 - factor(np-1);
deno = exp(temp);
vt = vt + (num./(deno+eps));
delta = abs(vt - vt0) * 10000.0;
vt0 = vt;
end
vt=vt(1);
if (np <= 50)
temp = vt./(1+snrbar);
c= gammainc(temp,np);%incomplete_gamma(temp,np);
pd = 1.0 - c;
%return
else
temp1 = snrbar + 1.0;
omegabar = sqrt(np) * temp1;
c3 = -1.0 / sqrt(np);
c4 = 1/(4*np);
c6 = (c3 * c3) /2.0;
V = (vt - (np * temp1)) / omegabar;
Vsqr = V *V;
val1 = exp(-Vsqr / 2.0) / sqrt( 2.0 * pi);
val2 = c3 * (V^2 -1.0) + c4 * V * (3.0 - V^2) -(c6 * V * (V^4 - 10. *
V^2 + 15.0));
q = 0.5 * erfc (V/sqrt(2.0));
pd = q - val1 * val2
end
%plot(snrbar1,pd)
xlabel('SNR dB')
ylabel('Probability of Detection')


M=0:40;% Cell array
cfar=-(5./M)*log10(pfa);
plot(c,cfar,'r')
%xlabel('Probability of Detection')
%ylabel('CFAR')
%plot(snrbar1,cfar,'r')




xlabel('Gamma Function')
ylabel('CFAR')
title('CFAR vs Gamma Function for Swerling 2')
```